European Journal of Protistology
April 2022, Volume 83, Pages 125875 (21p.)
https://doi.org/10.1016/j.ejop.2022.125875
https://archimer.ifremer.fr/doc/00751/86257/

First insights on the diversity of the genus *Ostreopsis* (Dinophyceae, Gonyaulacales) in guadeloupe island, with emphasis on the phylogenetic position of *O. heptagona*

Boisnoir Aurélie [1], Bilien Gwenael [2], Lemée Rodolphe [3], Chomérat Nicolas [2, *]

[1] Ifremer, BIODIVENV, F-97231 Le Robert, Martinique, France
[2] Ifremer, LITTORAL, F-29900 Concarneau, France
[3] Sorbonne Université, CNRS, Laboratoire d'Océanographie de Villefranche, Villefranche-sur-Mer, France

* Corresponding author : Nicolas Chomérat, email address : nicolas.chomerat@ifremer.fr

Abstract :

The present study aims to identify epiphytic Ostreopsis cells collected in Guadeloupe between 2017 and 2018 using a morpho-molecular approach. This method combined microscopical observations of wild specimens (light and scanning electron microscopy) with a phylogenetic analysis inferred from concatenated sequences of ribosomal operon (SSU + ITS + LSU) of Ostreopsidoideae. Four distinct morphotypes were identified in our samples and studied by SEM. Molecular data obtained from single-cell PCR for the four morphotypes were consistent with observations and confirmed the presence of three Ostreopsis species resolved in well characterized genotypes (O. cf. ovata, O. lenticularis and O. siamensis) and an unidentified clade. Detailed morphological characters including sulcal plates confirmed the identification of the last morphotype as O. heptagona D.R.Norris, J.W.Bomber & Balech, which forms a new basal clade in the genus, not previously reported. Observations highlighted overlapping sizes for O. lenticularis, O. siamensis and O. heptagona. Direct sequencing of PCR products obtained for some O. lenticularis and O. heptagona collected at one site revealed unexpectedly the presence of the parasitoid dinoflagellate Amoebophrya. Some Ostreopsis cells were found partially emptied and exhibiting a compact mass. Further analyses are needed to understand the ecological role of Amoebophrya on blooms of epiphytic Ostreopsis species.

Highlights

► Identification of four *Ostreopsis* species and characterization of a novel basal clade. ► Detailed SEM observations and rDNA sequencing of *Ostreopsis heptagona.* ► Detection of infected *Ostreopsis* spp. cells by the parasitoid *Amoebophrya.*

Keywords : Concatenated phylogeny, Morpho-molecular taxonomy, Ostreopsis cf. ovate, Ostreopsis lenticularis, Ostreopsis siamensis, Ribosomal operon

Introduction

The dinoflagellate genus *Ostreopsis* Johs.Schmidt, 1901 had first been observed in plankton samples collected in the Gulf of Thailand (Schmidt, 1901) but has seldomly been reported since then, due to its predominantly benthic habitat (Besada et al., 1982). Owing to its co-occurrence with the genus *Gambierdiscus* in tropical regions (Fukuyo, 1981; Ballantine et al., 1985; Berland et al., 1992), this genus benefited from the interest on microalgae associated with the ciguatera poisoning (CP) which allowed the description of several species between the 1980's and the 1990's (Fukuyo, 1981; Norris et al., 1985; Faust and Morton, 1995; Faust, 1999) and initiated the assessment of their toxicity (Ballantine et al., 1988; Tosteson et al., 1989; Berland et al., 1992). The toxins synthesized by *Ostreopsis* species are palytoxin-like molecules that can cause health issues especially in temperate areas (Gallitelli et al., 2005; e.g. Durando et al., 2007; Tichadou et al., 2010; Vila et al., 2016) where some species form recurrent blooms (Shears and Ross, 2009; Cohu et al., 2013; Ninčević Gladan et al., 2019; Açaf et al., 2020). Reports of *Ostreopsis* have become more and more frequent over the past decades (Shears and Ross, 2009; Shah et al., 2014; Park et al., 2020). Furthermore, palytoxin analogues can bio-accumulate in marine organisms (Biré et al., 2013, 2015) and constitute a significant risk for human health because of their potentially high toxicity and their thermostability (Katikou, 2007). Blooms are less frequently reported in tropical areas (Shears and Ross, 2009), but it has been shown that some species can reach high abundances and sometimes form benthic blooms (Chomérat et al., 2020b). Although palytoxin-like molecules have not been directly linked-with CP, they may be involved in poisoning derived from the ingestion of tropical marine organisms causing various symptoms reported in ciguateric endemic areas such as palytoxicosis and clupeotoxism (Alcala et al., 1988; Onuma et al., 1999; Randall, 2005).

In terms of species diversity, the Caribbean basin appears as a particularly rich area where nine of the eleven currently described species included in the genus *Ostreopsis* (Guiry and Guiry, 2021) have been reported from the Gulf of Mexico and the Caribbean Sea. Three species described from the Indo-Pacific area have been mentioned in the Caribbean, such as *O. siamensis* Johs.Schmidt (Bomber et al., 1988, 1989; Faust and Gulledge, 1996), *O. ovata* Y.Fukuyo (Besada et al., 1982; Faust and Gulledge, 1996; Faust, 2004) and *O. lenticularis* Y.Fukuyo (Ballantine et al., 1985, 1988; Tosteson et al., 1986, 1989; Faust, 1995, 2004; Faust et al., 1996; Delgado et al., 2006). Interestingly, five other species have been described from various areas of the Caribbean basin, including *O. heptagona* D.R.Norris, J.W.Bomber & Balech (Norris et al., 1985), *O. labens* M.A.Faust & S.L.Morton (Faust and Morton, 1995), *O. belizeana* M.A.Faust, *O. caribbeana* M.A.Faust and *O. marina* M.A.Faust (Faust, 1999). While the presence of *O. heptagona, O. labens* and *O. mascarenensis* Quod (Quod, 1994) has been suggested in various tropical areas (Faust and Morton, 1995; Faust et al., 1996), the other three species have never been unambiguously identified elsewhere than in their type localities. For instance the putative identification of *O. marina* in the

Indian Ocean (Carnicer et al., 2015) was unclear, and morphological and genetic data allowed to conclude that the species present in that region actually belongs to *O. lenticularis* (Chomérat et al., 2019b).

As stated previously, the morphological plasticity in *Ostreopsis* species led to some ambiguous identifications (Parsons et al., 2012; Hoppenrath et al., 2014; Chomérat et al., 2019b; Rhodes et al., 2020) and the existence of some *Ostreopsis* morphospecies has recently been questioned (Borsato et al., 2020; Chomérat et al., 2020b). In the Caribbean area, health risks associated with the toxicity of some *Ostreopsis* species have been reported (Norris et al., 1985; Tosteson et al., 1986; e.g. Ballantine et al., 1988), the identification of toxic species, however, remained unclear (Chomérat et al., 2019b), and further studies based on molecular data appear now necessary to resolve such issues (Sato et al., 2011; Tawong et al., 2014; Zhang et al., 2018). The use of molecular data from ribosomal DNA or internal transcribed spacers regions has proven to be extremely powerful to discriminate genotypes within the genus (e.g Penna et al., 2010; Sato et al., 2011; Tawong et al., 2014; Lee and Park, 2020). Still, association of genotypes with existing taxonomic descriptions was not always clear, since morphological data were lacking or not detailed enough for accurate characterization (Sato et al., 2011; Chomérat et al., 2020b). Only two species, *O. fattorussoi* Accoroni, Romagnoli & Totti and *O. rhodesiae* Verma, Hoppenrath & S.A.Murray include molecular data with their formal description (Accoroni et al., 2016; Verma et al., 2016), and recent re-investigations of *O. lenticularis*, *O. mascarenensis* and *O. siamensis* allowed to clarify their genetic identity (Chomérat et al., 2019b, 2020a; Nguyen-Ngoc et al., 2021). Combining morphological and genetic data from specimens acquired at or near the type localities appears as a major task to provide reliable taxonomic reference data for unambiguous identification of species (Parsons et al., 2012).

To date, there are no molecular studies on the genus *Ostreopsis* available from the Caribbean and there is a serious need of data to confirm the putatively high diversity inferred from morphological reports. Therefore, in the framework of a program aiming to explore the diversity of benthic dinoflagellates in the Caribbean Sea, the present study focuses on clarifying the taxonomic diversity of *Ostreopsis* in Guadeloupe Island based on a morpho-genetic approach. For the first time, single-cells of different morphotypes isolated from samples collected around the island were used for molecular sequencing of LSU rDNA. In addition, detailed morphological features were studied with high resolution scanning electron microscopy to assess species identifications. By combining morphological and molecular data, the present study allowed to better interpret the diversity around Guadeloupe Island, which constitutes a prerequisite for ecological studies of benthic communities associated with CP. Moreover, this study showed, in an unexpected manner, the infection of *Ostreopsis* cells by the parasitoid *Amoebophrya*.

Material and Methods

Sampling

Samples were collected between July and October 2017 and in July 2018 at four sites in various parts of Guadeloupe Island: Bois Jolan, Chapelle, Le Gosier and Rivière Sens (Fig. 1). During the sampling, several macrophytes were carefully collected with surrounding water in 50 ml plastic tubes avoiding the resuspension of epiphytic microalgae growing on the thalli (Table 1). Acidic Lugol solution at 1% (v/v) was added to all samples to preserve the microalgae and 10 seconds agitation allowed benthic dinoflagellates to detach from the macrophyte (Jauzein et al., 2018). Then, the epiphytic suspension was passed through a 500 µm mesh to remove larger organisms and detritus. Samples were stocked in the dark at 4°C.

Light and scanning electron microscopy

For scanning electron microscopy (SEM), cells were first individually isolated and concentrated in 2 ml tubes containing water and a drop of formaldehyde to prevent the development of fungi. Then, cells were filtered on polycarbonate membrane filters (Millipore RTTP Isopore, 1.2 µm pore size, Millipore, Billerica, USA), rinsed in deionized water, and prepared according to Chomérat & Couté (2008). Dehydration was carried out in ethanol baths 15%, 30%, 50%, 70%, 95% vol. ethanol for about 20 min in each bath, and then several baths of absolute ethanol. Cells were then dried using an EMS 850 (Electron Microscopy Science, Hatfield, PA, USA) critical point drier. After gold-coating as in Chomérat et al. (2020b), SEM examinations were carried out using a Sigma 300 field-emission SEM (Carl Zeiss Microscopy GmbH, Jena, Germany) in full vacuum mode and with an electron acceleration of 2 kV. Cells were measured on SEM digital micrographs using ImageJ software (Rasband, 1997). Depth corresponds to dorso-ventral length (DV) and height to antero-posterior (AP) length. SEM images were presented on a uniform background using GNU Image Manipulation Program v.2.10.18. For dissection of thecal plates, isolated cells were placed in a small drap of water on a slide, covered with a coverslip, and a drop of sodium hypochlorite (5% final concentration) was deposited on the border. The coverslip was then gently pressed using a stick and dissociated thecal plates were observed at high magnification using a BX41 (Olympus, Tokyo, Japan) upright microscope equipped with DIC optics. The terminology used for thecal plates in this paper follows the hybrid system of Hoppenrath et al. (2014) and Norris et al. (1985) for some sulcal plates.

Single-cells isolation, DNA amplifications and sequencing

For molecular characterization, single-cells were isolated from preserved field-samples as described in Chomérat et al. (2019a). In order to focus on the diversity of *Ostreopsis* species in each site,

samples were analysed by sampling site, indistinctively of the macrophyte substratum. To resuspend epiphytic cells, the tube containing Lugol-fixed material was vigorously shaken and a subsample of 30 µl was diluted in 4 ml of filtered seawater in a small Petri dish. Each cell of interest was isolated with a micropipette under an inverted microscope (Olympus IX51, Tokyo, Japan) measured and photographed with a camera (Olympus E–300 digital, Tokyo, Japan). Then, the cells were rinsed in four drops of distilled water before being transferred into a 200 µl PCR tube containing 5 µl of PCR grade distilled water. This process allowed to associate the morphology of a specimen with its sequence (Chomérat et al., 2019a). Tubes containing single-cells were stored at -20 °C until further analysis. A nested Polymerase chain reaction (PCR) was used for the amplification of one or two regions of the large subunit of ribosomal DNA (rDNA) (D1–D3 and D8–D10 domains). The first round of PCR used ITS-FW and RB primers (Table S1) then a second round of PCR was carried out using 1 µl of the amplicon produced in the first round, allowing the separate amplification of the D1–D3 and D8–D10 regions. PCR reactions were carried out in 20 µl using KOD Hot Start Master Mix (Novagen-Merck KgaA, Darmstadt, Germany), according to the manufacturer's instructions. The PCR cycling comprised an initial 2 min heating step at 95 °C to activate the polymerase, followed by 35 cycles of 95 °C for 20 s, 56 °C for 20 s, and 70 °C for 2 min. Primers used were D1R and D3B for D1–D3 domain and D8 and OstD10R for D8–D10 domain (Table S1). To obtain sequences of the parasitoid, a specific primer (AmoebR) has been designed from preliminary sequence results obtained with universal primers, and used to amplify specifically SSU–ITS region of the parasitoid (Table S1). PCR products were visualized on a 1% agarose gel after electrophoresis and the positive samples were purified using the ExoSAP-IT PCR Product Cleanup reagent (Affymetrix, Cleveland, OH, USA).

To confirm parasitoid and host sequences from infected specimens, a cloning step has been added. To allow a better ligation of the amplicon, the second PCR round was carried out using Taq polymerase (Promega PCR master mix) and primers ITS-FW–D3B with an initial 2 min heating step at 95 °C to activate the polymerase, followed by 20 cycles of 95 °C for 20 s, 60 °C for 20 s, and a final extension at 70 °C for 2 min. After confirmation by agarose gel electrophoresis, positive PCR products were purified using NucleoMag kit (Macherey-Nagel) and cloning was performed using pGEM®-T Easy Vector Systems kit and JM109 Competent Cells (Promega) according to the manufacturer's instructions. Positive clones were extracted with PureLink Quick Plasmid Miniprep kit (Invitrogen).

The Big Dye Terminator v3.1 Cycle Sequencing Kit (Applied Biosystems, Tokyo, Japan) was used for sequencing purified PCR products. Primers and excess dye-labeled nucleotides were first removed using the Big Dye X-terminator purification kit (Applied Biosystems, Foster City, CA, USA). Sequencing products were run on an ABI PRISM 3130 Genetic Analyzer (Applied Biosystems). Forward and reverse reads were obtained.

Sequences alignment and phylogenetic analyses

Ostreopsis sequences of the LSU D1-D3, D8-10 and additionally ITS region for morphotype 4 acquired in the present study were used a in a multi-loci phylogenetic analysis following the most recent taxonomic treatment of gonyaulaceans by Tillmann et al. (2021), and including sequences of the three genera encompassed in subfamily Ostreopsidoideae Gottschling, Tillmann and Elbrächter. For that purpose, 138 sequences of *Ostreopsis* spp., *Coolia* spp. and *Alexandrium* spp. from the analysis by Tillmann et al. (2021) served as a basis to construct our matrix, using *Triadinium polyedricum* (2 sequences) and *Pyrodinium bahamense* (3 sequences) as outgroup. Sequences acquired on 25 different specimens in the present study and 21 *Ostreopsis* spp. sequences retrieved from GenBank were added to complete the genus diversity. Full voucher information of the systematically representative set comprising 184 gonyaulacean Ostreopsidoideae (84 *Ostreopsis* spp., 30 *Coolia* spp., 70 *Alexandrium* spp.) and outgroup (2 Gambierdiscoideae Fensome, F.J.R.Taylor, G.Norris, Sarjeant, Wharton & G.L.William , 3 Pyrodinioideae F.J.R.Taylor, G.Norris, Sarjeant, Wharton & G.L.William) are provided in Table S2. As described in Tillmann et al. (2021), for alignment constitution, separate matrices of the rRNA operon (i.e. SSU, ITS region and LSU) were constructed, aligned using MAFFT v. 7 (Katoh and Standley, 2013) and concatenated afterwards using Seaview v. 5.05 software (Gouy et al., 2010). After concatenation, the matrix was refined by eye with Linux version of MEGA software v. 10.1.7 (Kumar et al., 2018).

A second dataset was prepared to analyse the phylogenetic position of the parasitoid *Amoebophrya* sp. infecting some *Ostreopsis* specimens. A matrix including small subunit of ribosomal RNA (SSU) and internal transcribed spacer 1 was prepared, using closely related sequences retrieved in GenBank, some sequences covering only SSU. They were aligned with MUSCLE algorithm (Edgar, 2004) followed by refinement by eye.

Prior to phylogenetic analyses, jModeltest2 v. 2.1.7 (Darriba et al., 2012) was used to search for the most appropriate model of sequence evolution. Two methods of phylogenetic reconstruction were used. Maximum Likelihood analysis (ML) was performed using PHY-ML v. 3 software (Guindon et al., 2010), and a bootstrap analysis (500 pseudoreplicates) were to assess the relative robustness of branches of the ML tree. Bayesian Inference analysis (BI) was carried out using MrBayes 3.1.2 software (Ronquist and Huelsenbeck, 2003). Parameters used to run phylogenetic calculations are given in supplementary Table S3. Nomenclature of clades (genotypes) follows that proposed by Sato et al. (2011) and subsequently by Tawong et al. (2014) and Chomérat et al. (2019b, 2020b).

Results

Morphological observations

Based on their size and appearance, assignment to four distinct morphotypes was possible. Cells of the morphotype 1 were small and conspicuously tear-shaped (Figs 2, 3A–B, 7A). The morphotype 2 included broadly large oval cells with a regular margin (Figs 2, 3 –I, 7B–E) while the morphotype 3 corresponded to cells with a similar size and shape as morphotype 2 but with an irregular undulated margin and a twisted aspect (Figs 2, 4A–B, 7F–J). Finally, cells of morphotype 4 were large and tear-shaped (Figs 2, 5A–B, 6A, 7K–O). Morphotype 2 was found at CH, BJ and RS sites, morphotype 3 was only found at GO and RS sites, while morphotypes 1 and 4 were only present at RS and CH sites, respectively. Owing to these morphological peculiarities and their observation at certain stations, cells of the four morphotypes could be retrieved in the samples analysed by SEM, allowing further detailed observations of their characters. All cells were found to possess the typical plate pattern of the genus *Ostreopsis,* APC 3′ 7″ 6?c ?s 5‴ 2‴′. In the following descriptions, only significant distinctive morphological features are emphasized for each morphotype.

Morphotype 1 - *Ostreopsis* cf. *ovata* Y. Fukuyo

Cells were ovate (Figs 3A–B, 7A), 43.2−52.3 µm (mean ± SD: 48.1 ± 3.5 µm, n = 10) deep (dorso-ventral length), 24.1−34.4 µm wide (mean 28.2 ± 3.0 µm, n = 10). The length to width ratio varied from 1.52 to 1.87 (mean 1.71, n = 10) (Figs 3A– B). The apical pore complex (APC) was composed of a slightly curved Po plate of about 8 µm that was supported by a long 2′ plate reaching the 4″ plate dorsally (Fig. 3C). The cingulum was almost straight and deep (Figs 3D–E). The thecal surface was smooth and covered by thecal pores of 0.25−0.32 µm in diameter without collar rim (Figs 3F–G). Interestingly, some rare smaller thecal pores (*ca.* 50 nm in diameter) were visible on the surface of plates (Figs 3F–G).

Morphotype 2 - *Ostreopsis lenticularis* Y. Fukuyo

Cells were large, lenticulate in shape and broadly ovate (Figs 3H–I, 7B). Cells were 65.0−119.9 µm deep (mean ± SD: 95.8 ± 12.8 µm, n = 25) and 56.2−96.9 µm wide (mean ± SD: 77.8 ± 11.2 µm, n = 25). The length to width ratio varied from 1.11 to 1.39 (mean ± SD: 1.23 ± 0.08, n = 25). The APC was composed of a slightly curved Po plate of 15.8−18.2 µm (mean ± SD: 17.0 ± 1.2 µm, n = 5) (Fig. 3J). The first apical plate 1′ was rather large and six-sided (Fig. 5H). The second apical plate 2′ was short and did not reach the 4″ plate (Fig. 3J) . The cingulum was straight in lateral view (Figs 3K–L). The thecal surface was covered with two kinds of pores without collar rim (Fig. 3M). The large pores were 0.3−0.4 µm in diameter and the small pores were 90−150 nm in diameter. They were both present densely on the thecal surface.

Morphotype 3 - *Ostreopsis siamensis* Jons. Schmidt

Cells were broadly ovoidal (Figs 4A–B, 7F). They were 58.6−97.6 µm deep (mean ± SD: 80.4 ± 11.1 µm, n = 16) and 43.3−82.5 µm wide (mean ± SD: 66.1 ± 11.7 µm, n = 16). The length to width ratio varied from 1.04 to 1.50 (mean: 1.23, n = 16). The APC was composed of a slightly curved Po plate whose length varied from 14.8 to 17.9 µm (mean ± SD: 16.8 ± 1.0 µm, n = 8) (Fig. 4C). The first apical plate was six-sided (Fig. 4A).. The second apical plate 2′ was narrow, extending to contact the 4″ plate (Fig. 4C). Ventrally, the cingulum appeared oblique and formed a V-shape (Fig. 4D). Cells appeared bulging in the median part of the epitheca (height: 30.6–41.7 µm, n = 5) and thinner near the edges (Figs 4E−F, G). In lateral view, the cingulum was conspicuously undulated, giving a somewhat twisted aspect to the cells (Figs 4E−F). In the sulcal area, cells exhibited the ventral opening (Vo), the anterior left sulcal plate (Ssa), the anterior right sulcal plate (Sda) and the posterior sulcal plate (Sp) (Fig. 4H). On the hypotheca, plate 2‴′ had typical curved shape (Figs 6B, F) due to the cell twist. The thecal surface was covered with large pores (*ca.* 0.3 µm in diameter) surrounded by a shallow elevated rim and some very small pores (*ca.* 50–60 nm in diameter) were also present at a lower density (Fig. 4I).

Morphotype 4 - *Ostreopsis heptagona* D.R.Norris, J.W.Bomber & Balech

Cells were large, and typically tear-shaped (Figs 5A−B, 6A, 7K− O, S1). They were 77.9−110.5 µm deep (mean ± SD: 95.1 ± 6.2 µm, n = 45) and 45.7−75.2 µm wide (mean ± SD: 60.0 ± 6.8 µm, n = 43). The length to width ratio varied from 1.39 to 1.80 (mean ± SD: 1.56; n = 43). The APC was composed with a slightly curved Po plate 14.6−17.2 µm long (mean ± SD: 16.1 ± 0.9 µm; n = 8) with the apical pore consisting in a slit encircled by a row of thecal pores partially visible (Figs 5D, 6B). The epithecal surface examination of this morphotype revealed a conspicuous seven-sided (i.e. heptagonal) 1′ plate making contacts with plates Po, 3′, 1″, 2″, 5″, 6″ and 7″ (Figs 5A, C). The second apical plate 2′ was narrow and elongated and reached the 4″ plate dorsally (Fig. 5D). Plate 3′ was pentagonal (Fig. 5A). Precingular plates were unequal in size, with plates of the right side (i.e. 4″, 5″, 6″ and 7″) higher than those of the left side (Figs 5A,F). On the left side, plate 3″ was the smaller of the series. Among precingular plates, 1″, 3″, 6″ and 7″ were four-sided, in contrast with 2″, 4″ and 5″ which were pentagonal.

The cingulum appeared almost closed and straight in all studied specimens, and no cingular plates could be distinguished in SEM (Figs 5E−F, S1). In LM, some cingular plates (c1; c2) appeared very narrow (Figs 6B, D, E). The sulcus was small and narrow (Figs 5F−G). Ventrally, the ventral opening (Vo) was visible in contact with 1″ plate (Figs 5F−G, 6A, D). From SEM observations, only three sulcal plates could be resolved and some were obscured by the overlap of 1‴′ plate (Fig. 5G). Observation of dissected cells at high magnification in LM allowed to complete

the sulcus description and four additional plates could be observed (Figs 6C−I). The most conspicuous plates both in LM and SEM were the anterior left sulcal plate (Ssa) which appeared elongated and in contact with Vo and 1″ on the epitheca, while it extended on the left within the cingular furrow (Figs 5G, 6D, H) and the anterior right sulcal (Sda), elongated located below Ssa and forming a prominent list (Figs 5G, 6D, H). These two plates had a complex three dimensional structure, and appeared conspicuously curved when seen from top (Figs 6D−E, H−I). On the left side of Ssa, a deeply recessed plate with a squared shape on the right and a rounded indentation with a thick edge on the left margin, was present and interpreted as a 't' plate (Fig. 6G). Just below this plate, a rectangular posterior left sulcal (Ssp) plate was observed in contact with Ssa, Sda (Fig. 6H). A small elongated and almost triangular (Fig. 6E) posterior right sulcal plate (Sdp) was in inserted bewteen Ssp and the posterior sulcal plate (Sp) which was six-sided, and with a hyaline part where it was overlapped by 1‴″ (Fig. 6F). Finally, the dissection revealed that a ring-shaped plate delimiting Vo could detach from the Ssa (Fig. 6I), and it could be interpreted as an anterior sulcal plate (Sa).

The hypotheca comprised seven major plates unequal in size (Fig. 5B). Seen antapically, the 2‴/3‴ and 4‴/5‴ sutures appeared roughly at the same level (Fig. 5B). Plate 1‴″ was in contact with 1‴, 2‴, 2‴″ and overlapped the sulcal area (Fig. 5B, G, S1). Plate 2‴ was pentagonal with contacts with 1‴, 3‴, 1‴″, 2‴″ plates and the cingulum. Furthermore, this plate was broader on its dorsal part, giving an asymmetrical shape (Fig. 5B, S1). Plates 3‴ and 4‴ were both four-sided and roughly of the same size (Fig. 5B, S1). Four-sided plate 5‴ had the most distinctive shape with its long and curved suture in contact with plate 2‴″ and its narrower size ventrally (Figs 5B, S1).

Interestingly, in the population from sample CH1, we noticed some variations of the hypothecal pattern of some specimens, while no variation was seen on epithecae. On these particular cells, a small extra plate was found on the ventral part of 2‴″ plate, in contact with 1‴″ and Sp plates (Fig. S1). Plate 2‴″ of these specimens appeared to be split obliquely on its ventral left side, with the larger part (2‴″α) dorsal and six sided, and the smaller part (2‴″β) ventral and four-sided and more or less reduced (Fig. S1).

The thecal surface was homogeneously covered with a single type of pores *ca*. 0.3−0.4 µm in diameter (Fig. 5H). Some larger pores up to 0.5 µm were occasionally observed on some specimens (e.g. on plates 2‴ and 3‴, Fig. 5B).

Single-cells isolation and phylogenetic analysis

For the phylogenetic analysis of Ostreopsidoideae, the alignment comprised 189 OTUs including 25 specimens from Guadeloupe Island (Figs 7A– O) and was 6382 bp (1896 + 815 + 3671) long including gaps. It comprised 631 + 637 + 1352 parsimony-informative sites and 3785 distinct PhyML alignment patterns.

The ML majority-rule consensus tree is shown on Fig. 8 and topologies were largely congruent regardless of whether ML or bayesian inference methods were used. The genus *Ostreopsis* was monophyletic and fully supported among other Ostreopsidoideae (Figs 8, S2). *Coolia* formed a sister clade to *Ostreopsis* while *Alexandrium* appeared more basal (Figs 8, S2). Among *Ostreopsis*, 13 major lineages that corresponded to established taxa at species rank were resolved and well to fully supported (Fig. 8):*O.* cf. *ovata*, *O. rhodesiae*, *O. mascarenensis*, *O. fattorussoi*, *O. lenticularis, O. siamensis, O. heptagona* and *Ostreopsis* sp. 1/2-4, 7-10 (Fig. 8). Sequences acquired from the four different morphotypes in the present study (Figs 7A–O) were resolved within four major clades (Fig. 8). One sequence was recovered in *O.* cf. *ovata* clade*,* 11 in *O. lenticularis* clade, 6 in *O. siamensis* clade, and 7 in *O. heptagona* clade. Sequences of *O.* cf. *ovata*, *O. lenticularis* and *O. siamensis* from Guadeloupe Island were closely related to sequences already available in GenBank and thus represent known genotypes (Fig. 8). Within *O. lenticularis* clade, all sequences from Guadeloupe Island were closely related to those from French Polynesia (type locality) (Fig. 8). Among sequences of *O. siamensis*, the 6 sequences from the present study were resolved with a strong support with sequences from the Gulf of Thailand (TF25OS, VNPQ218) and Tahiti Island (PNA19-6, PNA19-8 and IFR20-173). By contrast, sequences of *O. heptagona* were all similar and clustered in a new clade, sister of all other *Ostreopsis* lineages, which did not include any sequence from GenBank (Fig. 8). This clade was basal to all other *Ostreopsis* sequences but it was fully recovered within *Ostreopsis* genus based on the concatenated analysis (100BS, 1.00PP). Phylogenetic analyses inferred from single locus sequences (ITS and LSU D1-D3 + D8-D10) are given in supplementary figures S3 and S4. While the exact same position was found for this clade, the support was less robust than in the concatenated analysis presented herein.

Detection of infected **Ostreopsis** *spp. cells by the parasitoid* **Amoebophrya** *sp.*

Direct sequencing of PCR products obtained for some specimens from sample CH1 (Table 1) unexpectedly revealed the presence the parasitoid dinoflagellate genus *Amoebophrya* which has not been previously recognized when isolating single-cells. This preliminary result indicated a possible contamination or the presence of this parasitoid in the sample, but contamination was excluded as several independent PCR analyses revealed the same finding. Since partial LSU sequences obtained were not useful enough for identification and phylogenetic analysis of the parasitoid, a more thorough investigation has been undertaken to confirm this result. New specimens have been sought in the Lugol-fixed sample CH1 for amplification of SSU–ITS region. Observed carefully with light microscope, some *Ostreopsis* cells were found to have a peculiar appearance and seemed partially emptied with gaps in their cytoplasm, and they exhibited a compact mass, more or less developed and located dorsally (Figs 9A–F). This typical feature has been observed both in *O. lenticularis*

(Figs 9A–D) and *Ostreopsis heptagona* (Figs 9E–F). For putatively infected specimens of *O. lenticularis* (IFR18-618, IFR18-622, IFR18-624), only sequences of the parasitoid were obtained. In case of the specimen IFR17-685 of *Ostreopsis heptagona* (Fig. 7N), sequences of both the parasitoid and the host were obtained. The four sequences of *Amoebophrya* sp. infecting *Ostreopsis* spp. (accession numbers MW363873-MW363876) were identical. In the ML-tree (Fig. 10), they were resolved with strong support with the sequence MK752531.1 of an isolate (AT5) for which the host was not identified. From the phylogenetic analysis, it appeared that among the great genetic diversity within *Amoebophrya*, the parasitoid identified in this study belongs to a clade distantly related to other genotypes known to infect other planktonic dinoflagellates genera such as *Akashiwo*, *Alexandrium*, *Ceratium* (=*Tripos*), *Cochlodinium*, *Dinophysis*, *Gonyaulax*, *Gymnodinium*, *Karlodinium*, *Phalacroma*, *Prorocentrum* and *Scrippsiella* (Fig. 10).

Discussion

Phylogeny and species identities

Results from morphotype observations and phylogenetic analysis confirm the presence of four *Ostreopsis* species in the samples studied from Guadeloupe Island. The concatenated tree reveal a similar topology than found in the recent study by Tillmann et al. (2021), and *Ostreopsis* is a well resolved genus among subfamily Ostreopsidoideae. Within *Ostreopsis* clade, the topology is also congruent with previous studies based on single locus data (e.g. Chomérat et al., 2019b, 2020b; Sato et al., 2011; Tawong et al., 2014) and using a longer dataset provides a stronger support for several clades. While three of the genotypes from Guadeloupe Island cluster unambiguously within already known clades of *Ostreopsis* (*O.* cf. *ovata*; *O. lenticularis* and *O. siamensis*), the analysis reveals a novel basal clade not previously identified in any other study and for which the identity needs to be clarified.

As confirmed by molecular data, smaller cells of morphotype 1 correspond to *O.* cf. *ovata*, and compared with existing morphological data for *O.* cf. *ovata*, cells from Guadeloupe Island are in the size range reported for this species from various areas (e.g. Fukuyo, 1981; Penna et al., 2010; Zhang et al., 2018; Junqueira de Azevedo Tibiriçá et al., 2019; Nascimento et al., 2020). The detailed morphological analysis by SEM also confirms the plate pattern and characters observed previously (Fukuyo, 1981; Junqueira de Azevedo Tibiriçá et al., 2019). Nevertheless, observations at high magnification show the presence of very small thecal pores (*ca.* 50 nm) on the surface of thecal plates, as recently reported by Tibiriça et al. (2019). Hence, this confirms that this species possesses a few small pores, as in other species such as *O. lenticularis* (Fukuyo, 1981; Chomérat et al., 2019b), *O. rhodesiae* (Verma et al., 2016) or in *O. siamensis* (Chomérat et al., 2020b; Nguyen-Ngoc et al., 2021). These small pores are however rare and quite difficult to observe, and they may

be present in certain strains only, which may explain the variability reported in different studies (e.g. Hoppenrath et al., 2014). Genetically, the unique sequence from Guadeloupe is not identical with any strain from GenBank and it might constitute a different ribotype.

Cells of morphotype 2 identified as *O. lenticularis* have the typical morphology of this large species, with wide and sometimes almost round cells. The size variation observed in specimens from Guadeloupe is larger than reported in any other study, exceeding the ranges 60–100 µm in depth and 45–80 µm in width given by Fukuyo (1981) in the original description. Interestingly, Faust et al. (1996) reported larger sizes for *O. lenticularis*, although it was obviously misidentified as '*O. siamensis'*, as emphasized by Chomérat et al. (2019b). Using specimens from various populations worldwide including the Caribbean Sea, the Indian Ocean and the Japanese Pacific Ocean, these authors reported 108−123 µm in depth and 76−86 µm in width, but in absence of location data it is impossible to know if there was a pattern linked with geographical origin. From these values, the size variation appears quite low, in contrast with the observations by Zhang et al. (2018) who reported specimens 68.0−113.5 µm deep and 56.5−97.3 µm wide in their study from Hainan Island, or in the present study. Faust et al. (1996) apparently did not find cells smaller than 108 µm deep which is already a very large size for this species, compared with its original description (Fukuyo, 1981; Chomérat et al., 2019b). However, it is noteworthy that such large specimens as observed by Faust et al. (1996) are present in Guadeloupe Island, and the present study reveals that they are genetically identical to other sequences of *O. lenticularis*, which suggests that all belong to the same species. As mentioned by Fukuyo (1981) and later by Chomérat et al. (2019b), the major thecal characters of this species are a straight cingulum, and the typical presence of large and small pores, the latter being very abundant. All these features are present in the specimens from Guadeloupe Island and no difference has been found with other data.

The last species clearly identified by morphology (morphotype 3) and molecular data is *O. siamensis*, which has been recently reinvestigated by Nguyen-Ngoc et al. (2021). Prior to this study, this genotype was referred as to *Ostreopsis* sp. 6 (Sato et al., 2011; Tawong et al., 2014; e.g. Chomérat et al., 2020b; Lee and Park, 2020). Cells are large, undulated with a sigmoid cingulum and large thecal pores are surrounded by a shallow elevated rim (Chomérat et al., 2020b; Nguyen-Ngoc et al., 2021). All these features correspond well to the observations in Guadeloupe Island, but the cell undulation was even more pronounced, giving an asymmetrical shape of the cells, visible even with light microscope. Regarding size, cells from Guadeloupe Island are almost in the same range than in Tahiti Island (cells 58.0−82.5 µm deep and 45.7−61.2 µm wide), but larger specimens have been found in the present study. Compared with data for *O. siamensis* (excluding *O.* cf. *siamensis* which is another species, Chomérat et al. 2020b; Nguyen-Ngoc et al. 2021), cell sizes from Guadeloupe are remarkably similar to measurements given by Fukuyo (1981) from Japanese populations. Compared with data by Faust et al. (1996), considering the misidentification between

O. lenticularis and *O. siamensis* by these authors (Chomérat et al., 2020b), a wider size range is observed in Guadeloupe Island. However, if data of *O. labens* and *O. siamensis* in Faust & Morton (1995) and Faust et al. (1996), are merged to consider a single species, the resulting size range becomes remarkably similar with our data, with cells 65−98 µm deep and 57−80 µm wide. As already pointed out by Chomérat et al. (2020b), larger sizes reported by Faust & Morton (1995) for *O. labens* must be regarded cautiously as the sizes measured on some micrographs using scale bars are outside the range given in the text. In addition, Chomérat et al. (2020b) questioned the existence of *O. labens* because morphology was not significantly different from *O. siamensis*, but it may be cryptic and belongs to one of the subclades within *O. siamensis* (Chomérat et al., 2020b). Additional sequences from the Caribbean region are necessary to resolve this question and present data from Guadeloupe Island, eastern Caribbean, bring new elements to help clarifying this issue. The fact that all sequences obtained in this study are almost identical and cluster with strong support with sequences from the Gulf of Thailand (TF39OS, VNPQ218) and Tahiti Island indicate unambiguously that all belong to *O. siamensis* since strain VNPQ218 from Phu Quoc has been recently proposed as epitype by Nguyen-Ngoc et al. (2021). Nevertheless, a different genotype putatively corresponding to *O. labens* may be present in Belize and absent in Guadeloupe Island, and molecular data from Belize (type locality of *O. labens*) are absolutely necessary to clarify its existence or its junior synonymy with *O. siamensis*.

Identification of the morphotype 4 as O. heptagona

The morphology of morphotype 4 in Guadeloupe Island fits almost perfectly with the description of *O. heptagona* from Knight Key, Florida (Norris et al., 1985). Regarding size, Norris et al. (1985) described it as a large species, 96−122 µm (average 108 µm) deep and 62−84 µm (average 70 µm) wide. Cell sizes in the present study are in the same range, although no specimen reached the higher values reported by Norris et al. (1985), while smaller cells have been observed in Guadeloupe Island. By comparison, Faust et al. (1996) reported smaller cells of *O. heptagona* in Belize, where size was 80−108 µm deep and 46−59 µm wide, and their lower values are in agreement with smaller specimens in our observations. Overall morphology and plate pattern of cells from Guadeloupe Island are similar to the description by Norris et al. (1985). The most striking character of this species is the presence of a conspicuous suture between 1′ and 5″ plates, giving a heptagonal shape to 1′ plate. Although this pattern has sometimes also been observed in teratological specimens of cultured *O.* cf. *ovata* (Besada et al., 1982; Penna et al., 2010), our observations reveal that it is an unambiguous character in all observed specimens. The shape and the number of sulcal plates observed match with the description of *O. heptagona* made by Norris et al. (1985) which confirm the identification of this species. Another conspicuous feature is the very narrow cingulum, almost

closed, which is also a character mentioned by Norris et al. (1985) who reported a width of *ca.* 1.5−3.0 µm.

In contrast with *O. lenticularis* or *O. siamensis* recently observed in detail with SEM (Chomérat et al., 2019b, 2020b), the small posterior right sulcal plate (Sdp) which inserts between Sda and Sp plates has not been observed in any specimen from Guadeloupe Island, and if present, it is completely hidden by the overlap of 1′′′′ plate. Previous SEM observations of this species are scarce. Faust et al. (1996) provided illustrations showing only partially the morphology of *O. heptagona,* and they observed one type of thecal pores (0.3 µm in diameter) which is similar with our data. Surprisingly, Accoroni et al. (2020) recently mentioned the use of SEM for identification of this species in Florida, but they did not provide any image nor molecular data preventing from any comparison. From all aforementioned, morphological characters of cells from Guadeloupe Island are in good agreement with the description of *O. heptagona*, and to our knowledge, the present study is the first to combine detailed SEM observations and DNA sequences of this species. However, since our material from Guadeloupe Island was relatively distant from type locality (*ca.* 2,250 km southeast from Knight Key), it would be important to obtain sequences from this area.

Interestingly, our observations of many cells from the population of Chapelle sample reveal some specimens with an aberrant hypothecal pattern, in particular with a split 2′′′′ plate, which has not previously been reported from field specimens of *O. heptagona*. Variations in the thecal plate pattern of dinoflagellates and existence of split plates is not unusual and this has been mentioned in several genera (e.g. Besada et al., 1982; Chesnick and Cox, 1985; Chomérat and Couté, 2008). Such variations concern more generally the epitheca than the hypotheca that is generally considered as more stable (Chesnick and Cox, 1985), so the present result seems contradictory. Since the sample in which specimens with additional plates have been found is also containing numerous infected cells by the parasitoid *Amoebophrya* (Syndiniales), it can be hypothesized that thecal variations occur more frequently in parasited host cells, but further investigations would be necessary confirm this fact.

Diversity and comparison with data from the Caribbean

As discussed previously by Chomérat et al. (2019b), several confusions have been made regarding *O. siamensis* and *O. lenticularis* in different studies, and in most reports the correct identification was not ascertained. For instance, the name change from *O. siamensis* in Carlson (1984) to *O. lenticularis* in Carlson & Tindall (1985) in the interpretation of the same dataset introduced some confusions which have been encouraged by the speculative statement by Norris et al. (1985) who considered the two species as possibly conspecific without any detailed argument. Some subsequent reports from the Caribbean area (e.g. Ballantine et al., 1985; Tosteson et al., 1986, 1989) do not provide a clear identification of *Ostreopsis* species and the identity of the studied species remains in

question. It cannot be excluded that several co-existing species have been misidentified and referred as to a single name. In 1990, Tindall et al. (1990) examined toxic clonal strains from U.S. Virgin Islands ascribed to '*O. lenticularis*' with SEM and realized that morphologically cells better correspond with the description of *O. siamensis,* but considering that this species had not been mentioned from the Caribbean, they intentionally continued with the misidentification of *O. lenticularis,* making the identity of the toxic species doubtful. Interestingly, using LM only, Gamboa Márquez et al. (1994) were able to accurately identify both *O. siamensis* and *O. lenticularis* from Los Roques archipelago in the Caribbean Sea of Venezuela, and they precisely represented some differences such as the cingulum undulation and the long 2′ plate in *O. siamensis* which are absent in *O. lenticularis* (cf. Figs 14, 16. in Gamboa-Márquez et al. 1994). In spite of these differences, Faust et al. (1996) surprisingly made a major confusion between the two species in their taxonomic study and provided mistaken descriptions, perpetuating confusions between these species (Chomérat et al. 2019a, b). These studies however revealed a great diversity and emphasize the presence of both *O. siamensis* and *O. lenticularis* in Caribbean samples, which we can confirm in the present study using molecular data. On the light of this evidence, and since previous studies showed an absence of toxicity in *O. lenticularis* in contrast with *O. siamensis* (Sato et al., 2011; Chomérat et al., 2019b, 2020b), several reports of toxic '*O. lenticularis'* from the Caribbean (Tosteson et al., 1986; Ballantine et al., 1988; Mercado et al., 1994; Meunier et al., 1997; e.g. Ashton et al., 2003; Pérez-Guzmán et al., 2008) appear now doubtful and need to be reinvestigated.

Moreover, descriptions of morphospecies with poor morphological distinctive features have from the Caribbean added sources of confusions. For instance, the descriptions of *O. labens* (Faust and Morton, 1995)*, O. belizeana*, *O. caribbeana*, and *O. marina* (Faust, 1999) introduced new names in an existing context of confused taxonomy. Size ranges of these species considerably overlap with other species and considering large variations observed in populations observed in the present study, it cannot be excluded that some of these species are junior synonyms of existing taxa, as aforementioned for *O. labens*, likely a synonym for *O. siamensis.* A similar situation occurs with *O. marina* which does not seem to be different from *O. lenticularis* except that it has a larger size, as putatively identified by Irola-Sansores et al. (2018). Molecular data from the present study reveal that larger specimens with this morphology are genetically identical with *O. lenticularis*, making the existence of *O. marina* as a separate species in question.

Reports of *O. ovata* all over the Caribbean [St. Barthelemy Island Besada et al.(1982); Virgin Islands, Carlson (1984); Venezuela, Gamboa Márquez et al. (1994); Belize and Puerto Rico, Faust et al. (1996), Cuba, Delgado et al. (2006)] are based exclusively on morphology. Nevertheless, recent studies demonstrated that morphology of *O.* cf. *ovata* is not distinctive and divergent genotypes such as *O.* cf. *ovata* complex (Nascimento et al., 2020), *Ostreopsis* sp. 1 (Sato et al., 2011) or *Ostreopsis* sp. 7 (Tawong et al., 2014) are cryptic. Hence our molecular

characterization confirms the presence of a genotype of the *O.* cf. *ovata* complex in Guadeloupe Island, but, as it was infrequently found only at Rivière Sens, other genotypes may be present in other sites. In contrast with larger species such as *O. lenticularis* and *O. siamensis*, this species received little attention in the Caribbean area, probably because it was less abundant (Carlson, 1984) and it has not been studied thoroughly. Since *O.* cf. *ovata* is now a widely common species worldwide, with some strains producing high levels of toxins (e.g. Nascimento et al., 2012; Tartaglione et al., 2017) causing health concerns and beaches closures (Tester et al., 2020), studies focussing on its genetics, distribution and potential toxicity should be further addressed in Guadeloupe Island and more generally in the Caribbean Sea.

By contrast, *O. heptagona* has been mentioned several times in the Gulf of Mexico where it has been originally described (Norris et al., 1985; Bomber et al., 1988, 1989; Okolodkov et al., 2007, 2014; Aguilar-Trujillo et al., 2017) and in the Caribbean area (Faust et al., 1996; Morton and Faust, 1997; Almazán-Becerril et al., 2015; Irola-Sansores et al., 2018). The presence of *O. heptagona* in Guadeloupe Island constitutes the southernmost report to date. In spite of its regular presence in various parts of this area, the potential toxicity of this species remains unclear, and the limited toxicity to mice assessed with an unclear LD50 > 5×10^6 cells·kg^{-1} (according to Babinchak in Norris et al. 1985) needs to be re-evaluated.

Species identification is hardly possible by light microscopy due to large variations in size. Poor distinctive morphological characters lead to considerable confusions in the past and the use of new identification tools based on molecular data appears to be essential for ecological studies and monitoring purposes. This work is however essential to generate a reference dataset of sequences, which constitutes a prerequisite for further development of molecular techniques based on environmental DNA such as probes for fluorescent *in situ* hydridization assay (Pitz et al., 2021), RT-PCR assays and metabarcoding analyses. While light microscopic observations can accurately estimate the abundance of the genus *Ostreopsis* (Boisnoir et al., 2018, 2019, 2020) studying species distribution, dynamics and phenology will be facilitated by implementation of such tools at the scale of the Caribbean.

Evidence of parasitism on **Ostreopsis** *cells*

Parasitoids belonging to the genus *Amoebophrya* are known to infect various planktonic organisms such as radiolarians or dinoflagellate populations (Cachon, 1964) as *Akashiwo, Alexandrium, Ceratium, Cochlodinium, Dinophysis, Gymnodinium*, *Gyrodinium, Karlodinium*, *Phalacroma*, *Prorocentrum*, and *Scrippsiella* (Coats and Park, 2002; Chambouvet et al., 2008; Chambouvet, 2009; Alves-de-Souza et al., 2012). Interestingly, and in spite of being described as a generalist parasitoid which can infect a great variety of hosts, *Ostreopsis* species have never been associated with *Amoebophrya* infection, and thus present data constitute the first evidence that such events

occur in natural populations. From our data, the same parasitoid species can infect at least two different *Ostreopsis* species, namely *O. lenticularis* and *O. heptagona,* which confirms a low specificity. The compact mass within dinoflagellate cells could correspond to the trophont stage, an advanced stage of the infection caused by the parasitoid *Amoebophrya* (Cachon, 1964; Chambouvet et al., 2008). In addition, infections of other dinoflagellate genera present in the same samples (e.g. *Gambierdiscus* spp., *Prorocentrum* spp.) have not been investigated and are possible. From a molecular point of view, the genotype of the parasitoid found in the present study is rather distant from *Amoebophrya* strains isolated from other dinoflagellates and only one sequence of this genotype was already available in GenBank (MK752531, *Amoebophrya* sp. isolate AT5), without any indication of the putative host and origin.

This unexpected finding is an illustration of serendipity, and as it was not the focus of the study, several aspects regarding parasitism remain in question due to inappropriate sampling. The presence of *Amoeboprhrya* infecting populations of *Ostreopsis* spp. could impact their dynamics and probably constitute an important controlling factor of the blooms (Chambouvet et al., 2008; Mazzillo et al., 2011; Park et al., 2019). Further analyses should focus on determining the host specificity, the prevalence/infectivity, and the generation time of *Amoebophrya* sp. (Coats and Park, 2002). As suggested by Kim and Park (2016), parasitism may play a role in the toxicity of dinoflagellates, and such interactions should probably better taken into consideration in studies of benthic toxigenic taxa.

Acknowledgments

The authors extend special to thanks to Dr. Marc Gottshling for his advices regarding phylogenetic analysis and for sharing his alignment of gonyaulacean dinophytes, and to Dr Philipp Hess for editing of the English language. Authors acknowledge the support of the Collectivité Territoriale de Martinique for allowing this project been carried out.

AB wishes to express her deep gratitude to the GDR Phycotox and the members of the Club Soroptimist Diamant Les Rivières. The Regional Council of Brittany, the General Council of Finistère, the urban community of Concarneau Cornouaille Agglomération and the European Regional Development Fund (ERDF) are acknowledged for the funding of the Sigma 300 FE-SEM of the Concarneau Marine Biology Station.

Disclosure statement

No potential conflict of interest was reported by the authors.

Funding

This work is part of CARTAGO project and was supported by funds of the GDR Phycotox (Ifremer / CNRS 3659 research network on HABs) and the scholarship of Soroptimist-Union française.

Authors contributions

A. Boisnoir: original concept, sampling, microscopy, drafting and editing manuscript; G. Bilien: molecular analysis, sequencing and editing manuscript, R. Lemée: original concept, editing manuscript; N. Chomérat: original concept, microscopy, analysis of molecular data, drafting and editing manuscript.

References

Açaf, L., Abboud-Abi Saab, M., Khoury-Hanna, M., Lemée, R., 2020. Bloom dynamics of the newly described toxic benthic dinoflagellate *Ostreopsis fattorussoi* along the Lebanese coast (Eastern Mediterranean). Reg. Stud. Mar. Sci. 38, 101338.

Accoroni, S., Romagnoli, T., Penna, A., Capellacci, S., Ciminiello, P., Dell'Aversano, C., Tartaglione, L., Saab, M.A.-A., Giussani, V., Asnaghi, V., Chiantore, M., Totti, C., 2016. *Ostreopsis fattorussoi* sp. nov. (Dinophyceae), a new benthic toxic *Ostreopsis* species from the eastern Mediterranean Sea. J. Phycol. 52, 1064–1084.

Accoroni, S., Totti, C., Romagnoli, T., Giulietti, S., Glibert, P.M., 2020. Distribution and potential toxicity of benthic harmful dinoflagellates in waters of Florida Bay and the Florida Keys. Mar. Environ. Res. 155, 104891.

Aguilar-Trujillo, A.C., Okolodkov, Y.B., Herrera-Silveira, J.A., Merino-Virgilio, F. del C., Galicia-García, C., 2017. Taxocoenosis of epibenthic dinoflagellates in the coastal waters of the northern Yucatan Peninsula before and after the harmful algal bloom event in 2011–2012. Mar. Pollut. Bull. 119, 396–406.

Alcala, A.C., Alcala, L.C., Garth, J.S., Yasumura, D., Yasumoto, T., 1988. Human fatality due to ingestion of the crab *Demania reynaudii* that contained a palytoxin-like toxin. Toxicon 26, 105–107.

Almazán-Becerril, A., Escobar-Morales, S., Rosiles-González, G., Valadez, F., 2015. Benthic-epiphytic dinoflagellates from the northern portion of the Mesoamerican Reef System. Bot. Mar. 58, 115–128.

Alves-de-Souza, C., Varela, D., Iriarte, J.L., González, H.E., Guillou, L., 2012. Infection dynamics of Amoebophryidae parasitoids on harmful dinoflagellates in a southern Chilean fjord dominated by diatoms. Aquat. Microb. Ecol. 66, 183–197.

Ashton, M., Tosteson, T., Tosteson, C., 2003. The effect of elevated temperature on the toxicity of the laboratory cultured dinoflagellate *Ostreopsis lenticularis* (Dinophyceae). Rev. Biol. Trop. 51, 1–6.

Ballantine, D.L., Bardales, A.T., Tosteson, C.G., 1985. Seasonal abundance of *Gambierdiscus toxicus* and *Ostreopsis* sp. in coastal waters of southwest Puerto-Rico, in: Proceeding of the Fifth International Coral Reef Congress. Tahiti, pp. 417–422.

Ballantine, D.L., Tosteson, T.R., Bardales, A.T., 1988. Population dynamics and toxicity of natural populations of benthic dinoflagellates in southwestern Puerto Rico. J. Exp. Mar. Biol. Ecol. 119, 201–212.

Berland, B., Grzebyk, D., Thomassin, B., 1992. Benthic dinoflagellates from the coral reef lagoon ecophysiological study. Bull. Société Pathol. Exot. 1990 85, 453–6.
Besada, E.G., Loeblich, L.A., Loeblich III, A.R., 1982. Observations on tropical, benthic dinoflagellates from ciguatera-endemic areas: *Coolia*, *Gambierdiscus*, and *Ostreopsis*. Bull. Mar. Sci. 32, 723–735.
Biré, R., Trotereau, S., Lemée, R., Delpont, C., Chabot, B., Aumond, Y., Krys, S., 2013. Occurrence of palytoxins in marine organisms from different trophic levels of the French Mediterranean coast harvested in 2009. Harmful Algae 28, 10–22.
Biré, R., Trotereau, S., Lemée, R., Oregioni, D., Delpont, C., Krys, S., Guérin, T., 2015. Hunt for palytoxins in a wide variety of marine organisms harvested in 2010 on the French Mediterranean coast. Mar. Drugs 13, 5425–5446.
Boisnoir, A., Pascal, P.-Y., Cordonnier, S., Lemée, R., 2018. Depth distribution of benthic dinoflagellates in the Caribbean Sea. J. Sea Res. 135, 74–83.
Boisnoir, A., Pascal, P.-Y., Cordonnier, S., Lemée, R., 2019. Spatio-temporal dynamics and biotic substrate preferences of benthic dinoflagellates in the Lesser Antilles, Caribbean sea. Harmful Algae 81, 18–29.
Boisnoir, A., Pascal, P.-Y., Chomérat, N., Lemée, R., 2020. Distribution of potentially toxic epiphytic dinoflagellates in Saint Martin Island (Caribbean Sea, Lesser Antilles). Cryptogam. Algol. 41, 47–54.
Bomber, J.W., Morton, S.L., Babinchak, J.A., Norris, D.R., Morton, J.G., 1988. Epiphytic dinoflagellates of drift algae — another toxigenic community in the Ciguatera Food Chain. Bull. Mar. Sci. 43, 204–214.
Bomber, J.W., Rubio, M.G., Norris, D.R., 1989. Epiphytism of dinoflagellates associated with the disease ciguatera: substrate specificity and nutrition. Phycologia 28, 360–368.
Borsato, G.T., Salgueiro, F., da Silva, C.G.T., Menezes-Salgueiro, A.D., Nascimento, S.M., 2020. *Ostreopsis lenticularis* Y. Fukuyo (Dinophyceae, Gonyaulacales) from the South Atlantic Ocean: morphological and molecular characterization. Mar. Pollut. Bull. 158, 111441.
Cachon, J., 1964. Contribution à l'étude des péridiniens parasites : Cytologie, cycles évolutifs. Ann. Sci. Nat. Zool. Biol. Anim. Serie 12, 1–158, pl. 1–36.
Carlson, R.D., 1984. Distribution, periodicity, and culture of benthic/epiphytic dinoflagellates in a ciguatera endemic region of the Caribbean. PhD Thesis. Southern Illinois University, Carbondale.
Carlson, R.D., Tindall, D.R., 1985. Distribution and periodicity of toxic dinoflagellates in the Virgin Islands., in: Proceeding of the Third International Conference on Toxic Dinoflagellates. Presented at the Toxic dinoflagellates, Anderson, DM, White, AW, Baden, DG (eds), pp. 171–176.
Carnicer, O., Tunin-Ley, A., Andree, K.B., Turquet, J., Diogène, J., Fernández-Tejedor, M., 2015. Contribution to the genus *Ostreopsis* in Reunion Island (Indian Ocean): molecular, morphologic and toxicity characterization. Cryptogam. Algol. 36, 101–119.
Chambouvet, A., Morin, P., Marie, D., Guillou, L., 2008. Control of toxic marine dinoflagellate blooms by serial parasitic killers. Science 322, 1254–1257.
Chambouvet, A., 2009. Les amoebophryidae (Syndiniales) parasitoïdes de dinoflagellés : cycle de vie, dynamique et spécificité in situ. Parasitologie. PhD thesis. Paris 6, France.
Chesnick, J.M., Cox, E.R., 1985. Thecal plate tabulation and variation in *Peridinium balticum* (Pyrrhophyta: Peridiniales). Trans. Am. Microsc. Soc. 104, 387–394.
Chomérat, N., Couté, A., 2008. *Protoperidinium bolmonense* sp. nov. (Peridiniales, Dinophyceae), a small dinoflagellate from a brackish hypereutrophic lagoon (South of France). Phycologia 47, 392–403.
Chomérat, N., Bilien, G., Zentz, F., 2019a. A taxonomical study of benthic *Prorocentrum* species (Prorocentrales, Dinophyceae) from Anse Dufour (Martinique Island, eastern Caribbean Sea). Mar. Biodivers. 49, 1299–1319.
Chomérat, N., Bilien, G., Derrien, A., Henry, K., Ung, A., Viallon, J., Darius, H.T., Mahana iti Gatti, C., Roué, M., Hervé, F., Réveillon, D., Amzil, Z., Chinain, M., 2019b. *Ostreopsis*

lenticularis Y. Fukuyo (Dinophyceae, Gonyaulacales) from French Polynesia (South Pacific 95–111.

Chomérat, N., Bilien, G., Couté, A., Quod, J.-P., 2020a. Reinvestigation of *Ostreopsis mascarenensis* Quod (Dinophyceae, Gonyaulacales) from Réunion Island (SW Indian Ocean): molecular phylogeny and emended description. Phycologia 59, 140–153.

Chomérat, N., Bilien, G., Viallon, J., Hervé, F., Réveillon, D., Henry, K., Zubia, M., Vieira, C., Ung, A., Gatti, C.M. iti, Roué, M., Derrien, A., Amzil, Z., Darius, H.T., Chinain, M., 2020b. Taxonomy and toxicity of a bloom-forming *Ostreopsis* species (Dinophyceae, Gonyaulacales) in Tahiti island (South Pacific Ocean): one step further towards resolving the identity of *O. siamensis*. Harmful Algae 98, 101888.

Coats, D.W., Park, M.G., 2002. Parasitism of photosynthetic dinoflagellates by three strains of *Amoebophrya* (dinophyta): parasite survival, infectivity, generation time, and host specificity. J. Phycol. 38, 520–528.

Cohu, S., Mangialajo, L., Thibaut, T., Blanfuné, A., Marro, S., Lemée, R., 2013. Proliferation of the toxic dinoflagellate *Ostreopsis* cf. *ovata* in relation to depth, biotic substrate and environmental factors in the North West Mediterranean Sea. Harmful Algae 24, 32–44.

Darriba, D., Taboada, G.L., Doallo, R., Posada, D., 2012. jModelTest 2: more models, new heuristics and parallel computing. Nat. Methods 9, 772–772.

Delgado, G., Lechuga-Devéze, C.H., Popowski, G., Troccoli, L., Salinas, C.A., 2006. Epiphytic dinoflagellates associated with ciguatera in the northwestern coast of Cuba. Rev. Biol. Trop. 54, 299–310.

Durando, P., Ansaldi, F., Oreste, P., Moscatelli, P., Marensi, L., Grillo, C., Gasparini, R., Icardi, G., 2007. *Ostreopsis ovata* and human health: Epidemiological and clinical features of respiratory syndrome outbreaks from a two year syndromic surveillance, 2005−2006, in northwest Italy. Eur. Commun. Dis. Bull. 12, E070607.1.

Edgar, R., 2004. MUSCLE: a multiple sequence alignment method with reduced time and space complexity. BMC Bioinformatics 5, 113.

Faust, M.A., 1995. Observation of sand-dwelling toxic dinoflagellates (dinophyceae) from widely differing sites, including two new species. J. Phycol. 31, 996–1003.

Faust, M.A., Morton, S.L., 1995. Morphology and ecology of the marine dinoflagellate *Ostreopsis labens* sp. nov. (dinophyceae). J. Phycol. 31, 456–463.

Faust, M.A., Gulledge, R.A., 1996. Associations of microalgae and meiofauna in floating detritus at a mangrove island, Twin Cays, Belize. J. Exp. Mar. Biol. Ecol. 197, 159–175.

Faust, M.A., Morton, S.L., Quod, J.P., 1996. Further SEM study of marine dinoflagellates: The genus *Ostreopsis* (Dinophyceae). J. Phycol. 32, 1053–1065.

Faust, M.A., 1999. Three new *Ostreopsis* species (Dinophyceae): *O. marinus* sp. nov., *O. belizeanus* sp. nov., and *O. caribbeanus* sp. nov. Phycologia 38, 92–99.

Faust, M.A., 2004. The dinoflagellates of Twin Cays, Belize: biodiversity, distribution and vulnerability. Atoll Res. Bull. 514, 1–20.

Fukuyo, Y., 1981. Taxonomical study on benthic dinoflagellates collected in coral reefs. Bull. Jpn. Soc. Sci. Fish. 47, 967–978.

Gallitelli, M., Ungaro, N., Addante, L.M., Procacci, V., Silver, N.G., Sabbà, C., 2005. Respiratory illness as a reaction to tropical algal blooms occurring in a temperate climate. J. Am. Med. Assoc. 293, 2595–2600.

Gamboa-Márquez, J., Sánchez Suárez, I., La Barbera Sánchez, A., 1994. Dinoflagelados (Pyrrhophyta) del archipielago Los Roques (Venezuela): familias Prorocentraceae y Ostreopsidaceae. Acta Científica Venez. 45, 140–52.

Gouy, M., Guindon, S., Gascuel, O., 2010. SeaView version 4: A multiplatform graphical user interface for sequence alignment and phylogenetic tree building. Mol. Biol. Evol. 27, 221–224.

Guindon, S., Dufayard, J.-F., Lefort, V., Anisimova, M., Hordijk, W., Gascuel, O., 2010. New algorithms and methods to estimate maximum-likelihood phylogenies: assessing the performance of PhyML 3.0. Syst. Biol. 59, 307–321.

Guiry, M.D., Guiry, G.M., 2021. *Algaebase*. World-wide electronic publication, National University Document]. URL (accessed 2.4.21).
Hoppenrath, M., Murray, S., Chomérat, N., Horiguchi, T., 2014. Marine benthic dinoflagellates - unveiling their worldwide biodiversity, Schweizerbart'sche Verlagbuchhandlung. ed. Kleine Senckenberg-Reihe, Germany.
Irola-Sansores, E.D., Delgado-Pech, B., García-Mendoza, E., Núñez-Vázquez, E.J., Olivos-Ortiz, A., Almazán-Becerril, A., 2018. Population dynamics of benthic-epiphytic dinoflagellates on two macroalgae from coral reef systems of the Northern Mexican Caribbean. Front. Mar. Sci. 5, 487.
Jauzein, C., Açaf, L., Accoroni, S., Asnaghi, V., Fricke, A., Hachani, M.A., Abboud-Abi Saab, M., Chiantore, M., Mangialajo, L., Totti, C., Zaghmouri, I., Lemée, R., 2018. Optimization of sampling, cell collection and counting for the monitoring of benthic harmful algal blooms: Application to *Ostreopsis* spp. blooms in the Mediterranean Sea. Ecol. Indic. 91, 116–127.
Junqueira de Azevedo Tibiriçá, C.E.J.A., Leite, I.P., Batista, T.V.V., Fernandes, L.F., Chomérat, N., Hervé, F., Hess, P., Mafra, L.L., 2019. *Ostreopsis* cf. *ovata* bloom in Currais, Brazil: phylogeny, toxin profile and contamination of mussels and marine plastic litter. Toxins 11, 446.
Katikou, P., 2007. Chemistry of Palytoxins and Ostreocins, in: Botana, L.M. (Ed.), Phycotoxins: Chemistry and Biochemistry. Blackwell Publishing, Ames, Iowa, USA, pp. 75–93.
Katoh, K., Standley, D.M., 2013. MAFFT Multiple sequence alignment software version 7: Improvements in performance and usability. Mol. Biol. Evol. 30, 772–780.
Kim, S., Park, M.G., 2016. Effect of the endoparasite *Amoebophrya* sp. on toxin content and composition in the paralytic shellfish poisoning dinoflagellate *Alexandrium fundyense* (Dinophyceae). Harmful Algae 51, 10–15.
Kumar, S., Stecher, G., Li, M., Knyaz, C., Tamura, K., 2018. MEGA X: Molecular evolutionary genetics analysis across computing platforms. Mol. Biol. Evol. 35, 1547–1549.
Lee, B., Park, M.G., 2020. Distribution and genetic diversity of the toxic benthic dinoflagellate genus *Ostreopsis* in Korea. Harmful Algae 96, 101820.
Mazzillo, F.F.M., Ryan, J.P., Silver, M.W., 2011. Parasitism as a biological control agent of dinoflagellate blooms in the California Current System. Harmful Algae 10, 763–773.
Mercado, J.A., Rivera-Rentas, A.L., Gonzalez, I., Tosteson, T.R., Molgó, J., Motta, G., 1994. Neuro-and myo-toxicity of extracts from the benthic dinoflagellate *Ostreopsis lenticularis* is sensitive to μ-conotoxin. Soc. Neurosci. Abstr. 20, 1224–1230.
Meunier, F.A., Mercado, J.A., Molgó, J., Tosteson, T.R., Escalona de Motta, G., 1997. Selective depolarization of the muscle membrane in frog nerve-muscle preparations by a chromatographically purified extract of the dinoflagellate *Ostreopsis lenticularis*. Br. J. Pharmacol. 121, 1224–1230.
Morton, S.L., Faust, M.A., 1997. Survey of toxic epiphytic dinoflagellates from the Belizean Barrier Reef Ecosystem. Bull. Mar. Sci. 61, 899–906.
Nascimento, S.M., Corrêa, E.V., Menezes, M., Varela, D., Paredes, J., Morris, S., 2012. Growth and toxin profile of *Ostreopsis* cf. *ovata* (Dinophyta) from Rio de Janeiro, Brazil. Harmful Algae 13, 1–9.
Nascimento, S.M., Neves, R.A.F., De'Carli, G.A.L., Borsato, G.T., da Silva, R.A.F., Melo, G.A., de Morais, A.M., Cockell, T.C., Fraga, S., Menezes-Salgueiro, A.D., Mafra, L.L., Hess, P., Salgueiro, F., 2020. *Ostreopsis* cf. *ovata* (Dinophyceae) molecular phylogeny, morphology, and detection of ovatoxins in strains and field samples from Brazil. Toxins 12, 70.
Nguyen-Ngoc, L., Doan-Nhu, H., Larsen, J., Phan-Tan, L., Nguyen, X.-V., Lundholm, N., Chu, T.V., Huynh-Thi, D.N., 2021. Morphological and genetic analyses of *Ostreopsis* (Dinophyceae, Gonyaulacales, Ostreopsidaceae) species from Vietnamese waters with a re-description of the type species, *O. siamensis*. J. Phycol.
Ninčević Gladan, Ž., Arapov, J., Casabianca, S., Penna, A., Honsell, G., Brovedani, V., Pelin, M., Tartaglione, L., Sosa, S., Dell'Aversano, C., Tubaro, A., Žuljević, A., Grbec, B., Čavar, M.,

Bužančić, M., Bakrač, A., Skejić, S., 2019. Massive occurrence of the harmful benthic
Norris, D.R., Bomber, J.W., Balech, E., 1985. Benthic dinoflagellates associated with ciguatera from the Florida Keys. I. *Ostreopsis heptagona* sp. nov., in: Toxic Dinoflagellates. D.M. Anderson, A.W. White & D.G. Baden, pp. 39–44.

Okolodkov, Y.B., Campos-Bautista, G., Gárate-Lizárraga, I., González-González, J.A.G., Hoppenrath, M., Arenas, V., 2007. Seasonal changes of benthic and epiphytic dinoflagellates in the Veracruz reef zone, Gulf of Mexico. Aquat. Microb. Ecol. 47, 223–237.

Okolodkov, Y.B., Merino-Virgilio, F. del C., Aké-Castillo, J.A., Aguilar-Trujillo, A.C., Espinosa-Matías, S., Herrera-Silveira, J.A., 2014. Seasonal changes in epiphytic dinoflagellate assemblages near the northern coast of the Yucatan Peninsula, Gulf of Mexico. Acta Bot. Mex. 107, 121–151.

Onuma, Y., Satake, M., Ukena, T., Roux, J., Chanteau, S., Rasolofonirina, N., Ratsimaloto, M., Naoki, H., Yasumoto, T., 1999. Identification of putative palytoxin as the cause of clupeotoxism. Toxicon 37, 55–65.

Park, B.S., Kim, S., Kim, J.-H., Ho Kim, J., Han, M.-S., 2019. Dynamics of *Amoebophrya* parasites during recurrent blooms of the ichthyotoxic dinoflagellate *Cochlodinium polykrikoides* in Korean coastal waters. Harmful Algae 84, 119–126.

Park, J., Hwang, J., Hyung, J.-H., Yoon, E.Y., 2020. Temporal and spatial distribution of the toxic epiphytic dinoflagellate *Ostreopsis* cf. *ovata* in the Coastal Waters off Jeju Island, Korea. Sustainability 12, 5864.

Parsons, M.L., Aligizaki, K., Bottein, M.-Y.D., Fraga, S., Morton, S.L., Penna, A., Rhodes, L., 2012. *Gambierdiscus* and *Ostreopsis*: Reassessment of the state of knowledge of their taxonomy, geography, ecophysiology, and toxicology. Harmful Algae, Harmful Algae--The requirement for species-specific information 14, 107–129.

Penna, A., Fraga, S., Battocchi, C., Casabianca, S., Giacobbe, M.G., Riobó, P., Vernesi, C., 2010. A phylogeographical study of the toxic benthic dinoflagellate genus *Ostreopsis* Schmidt. J. Biogeogr. 37, 830–841.

Pérez-Guzmán, L., Pérez-Matos, A.E., Rosado, W., Tosteson, T.R., Govind, N.S., 2008. Bacteria associated with toxic clonal cultures of the dinoflagellate *Ostreopsis lenticularis*. Mar. Biotechnol. 10, 492–496.

Pitz, K.J., Richlen, M.L., Fachon, E., Smith, T.B., Parsons, M.L., Anderson, D.M., 2021. Development of fluorescence in situ hybridization (FISH) probes to detect and enumerate *Gambierdiscus* species. Harmful Algae 101, 101914.

Quod, J.-P., 1994. *Ostreopsis mascarenensis* sp. nov (Dinophyceae) dinoflagellé toxique associéà la ciguatéra dans l'Océan Indien. Cryptogam. Algol. 243–252.

Randall, J.E., 2005. Review of clupeotoxism, an often fatal illness from the consumption of clupeoid fishes. Pac. Sci. 59, 73–77.

Rasband, W.S., 1997. ImageJ. Bethesda, National Institutes of Health, Maryland.

Rhodes, L.L., Smith, K.F., Murray, J.S., Nishimura, T., Finch, S.C., 2020. Ciguatera fish poisoning: The risk from an Aotearoa/New Zealand perspective. Toxins 12, 50.

Ronquist, F., Huelsenbeck, J.P., 2003. MrBayes 3: Bayesian phylogenetic inference under mixed models. Bioinformatics 19, 1572–1574.

Sato, S., Nishimura, T., Uehara, K., Sakanari, H., Tawong, W., Hariganeya, N., Smith, K., Rhodes, L., Yasumoto, T., Taira, Y., Suda, S., Yamaguchi, H., Adachi, M., 2011. Phylogeography of *Ostreopsis* along West Pacific coast, with special reference to a novel clade from Japan. Plos One 6, e27983.

Schmidt, J., 1901. Flora of Koh Chang. Contributions to the knowledge of the vegetation in the Gulf of Siam. Part IV. Peridiniales. J. Bot. 24, 212–221.

Shah, M.M.R., An, S.-J., Lee, J.-B., 2014. Occurrence of sand-dwelling and epiphytic dinoflagellates including potentially toxic species along the coast of Jeju island, Korea. J. Fish. Aquat. Sci. 9, 141–156.

Shears, N.T., Ross, P.M., 2009. Blooms of benthic dinoflagellates of the genus *Ostreopsis*; an worldwide. Harmful Algae 8, 916–925.

Tartaglione, L., Dello Iacovo, E., Mazzeo, A., Casabianca, S., Ciminiello, P., Penna, A., Dell'Aversano, C., 2017. Variability in toxin profiles of the Mediterranean *Ostreopsis* cf. *ovata* and in structural features of the produced Ovatoxins. Environ. Sci. Technol. 51, 13920–13928.

Tawong, W., Nishimura, T., Sakanari, H., Sato, S., Yamaguchi, H., Adachi, M., 2014. Distribution and molecular phylogeny of the dinoflagellate genus *Ostreopsis* in Thailand. Harmful Algae 37, 160–171.

Tester, P.A., Litaker, R.W., Berdalet, E., 2020. Climate change and harmful benthic microalgae. Harmful Algae 91, 101655.

Tichadou, L., Glaizal, M., Armengaud, A., Grossel, H., Lemée, R., Kantin, R., Lasalle, J.-L., Drouet, G., Rambaud, L., Malfait, P., de Haro, L., 2010. Health impact of unicellular algae of the *Ostreopsis* genus blooms in the Mediterranean Sea: experience of the French Mediterranean coast surveillance network from 2006 to 2009. Clin. Toxicol. Phila. Pa 48, 839–844.

Tillmann, U., Bantle, A., Krock, B., Elbrächter, M., Gottschling, M., 2021. Recommendations for epitypification of dinophytes exemplified by Lingulodinium polyedra and molecular phylogenetics of the Gonyaulacales based on curated rRNA sequence data. Harmful Algae 104, 101956.

Tindall, D.R., Miller, D.M., Tindall, P.M., 1990. Toxicity of *Ostreopsis lenticularis* from the British and United States Virgin Islands., in: Proceedings of the Fourth International Conference on Toxic Marine Phytoplankton. Presented at the Toxic Marine Phytoplankton, Lund, Sweden, pp. 424–429.

Tosteson, T.R., Ballantine, D.L., Tosteson, C.G., Bardales, A.T., Dust, H.D., Higert, T.B., 1986. Comparative toxicity of *Gambierdiscus toxicus*, *Ostreopsis* cf. *lenticularis* and associated microflora. Mar. Fish. Rev. 48, 57–59.

Tosteson, T.R., Ballantine, D.L., Tosteson, C.G., Hensley, V., Bardales, A.T., 1989. Associated bacterial flora, growth, and toxicity of cultured benthic dinoflagellates *Ostreopsis lenticularis* and *Gambierdiscus toxicus*. Appl. Environ. Microbiol. 55, 137–141.

Verma, A., Hoppenrath, M., Dorantes-Aranda, J.J., Harwood, D.T., Murray, S.A., 2016. Molecular and phylogenetic characterization of *Ostreopsis* (Dinophyceae) and the description of a new species, *Ostreopsis rhodesae* sp. nov., from a subtropical Australian lagoon. Harmful Algae 60, 116–130.

Vila, M., Abós-Herràndiz, R., Isern-Fontanet, J., Alvarez, J., Berdalet, E., 2016. Establishing the link between *Ostreopsis* cf. *ovata* blooms and human health impacts using ecology and epidemiology. Sci. Mar. 80, 107–115.

Zhang, H., Lu, S., Li, Y., Cen, J., Wang, H., Li, Q., Nie, X., 2018. Morphology and molecular phylogeny of *Ostreopsis* cf. *ovata* and *O. lenticularis* (Dinophyceae) from Hainan Island, South China Sea. Phycol. Res. 66, 3–14.

Figure legends

Fig. 1. Maps showing the location of Guadeloupe Island in the Caribbean Sea and sampling sites

Fig. 2. Size ranges observed for the four different morphotypes calculated using all available data from LM and SEM. Crosshairs show the minimum, maximum and mean (at intersection) values for depth (i.e. DV length) and width. Individual symbols correspond to single-cells used in the phylogenetic analysis (isolate numbers given in italics) and measured from LM.

Figs 3.A–M SEM micrographs of morphotype 1 (*O.* cf. *ovata*) from Rivière-Sens **(A–G)** and morphotype 2 (*O. lenticularis*) from Chapelle **(H–M)**. **A:** Apical view. **B:** Antapical view. **C:** Detail of 2′ and 3′ plates and apical pore complex (APC). **D:** Left latero-apical view. **E:** Right lateral view showing the straight cingulum. **F**–**G:** Detail of thecal pores, with some small pores (arrows) visible. **H:** Apical view. **I:** Antapical view. **J:.** Detail of 2′ (short) and 3′ plates and apical pore complex (APC). **K:** Left lateral view showing the straight cingulum. **L:** Right lateral view showing the straight cingulum. **M:.** Detail of the smooth thecal surface with thecal pores of two sizes classes. Bars: 10 µm **(A–B, H–I, K–L)**; 5 µm **(D–E)**; 2 µm **(C, J)**, 1 µm **(F, M)**; 200 nm **(G)**.

Figs 4. **A–I** SEM micrographs of morphotype 3 (*O. siamensis*) from Rivière-Sens. **A:** Apical view. **B:** Antapical view. **C:** Detail of 2′ and 3′ plates and apical pore complex (APC). **D:** Ventral view. **E:** Right lateral view showing the undulated cingulum. **F:** Oblique antapical view showing the strong undulation of a cell. **G:** Oblique apical view showing the cell undulation and depression of the hyptheca. **H:** Detail of the ventral area with the 'ventral opening' (Vo) and sulcal plates visible. **I:** Detail of cell surface with two kinds of thecal pores visible, the smaller indicated with arrows. Bars,10 µm **(A–B, D–G)**; 5 µm **(C)**; 2 µm **(H)**; 1 µm **(I)**.

Figs 5A–H SEM micrographs of morphotype 4 (*O. heptagona*) from Chapelle site. **A:** Apical view with the suture 1′/5″ highlighted (arrowhead). **B:** Antapical view. **C:** Detail of the seven-sided first apical plate 1′, note the sutures 1′/5″ (white arrowhead) and 5″/6″ (black arrowhead). **D:** Detail of the apical pore complex (APC) and long 2′ plate contacting 4″ plate. **E:** Left lateral view of a specimen showing the almost straight and narrow cingulum. **F:** Ventro-apical view. **G:** Detail of the sulcal area with the ventral opening (Vo) and three sulcal plates visible. **H:** Detail of cell surface with one type of thecal pores. Bars: 10 µm **(A–B, E–F)**; 5 µm **(C)**; 2 µm **(D–G)**; 1 µm **(H)**.

Figs 6.A–I Light micrographs of dissected cells and sulcal plates of morphotype 4 (*O. heptagona*) from Chapelle **A:** Apical view of an epitheca showing the peculiar shape of 1′ plate. **B:** Detail of Po

and 2′ plates. **C:** Detached sulcal area from a broken theca. **D–E:** Views of a sulcal area with different level of focus, showing some small plates Sp, Sdp and the complex three dimensional shape of Ssa and Sda. **F:** Detail of an isolated Sp (with a hyaline area) and 1′′′′. **G:** Detail of the 't' plate at the left end of Ssa. **H:** Isolated Ssa, Sda bearing a conspicuous list, and Ssp. **I:** Isolated Ssa and Sda with a detached annular platelet (Sa) encircling Vo. Bars: 20 µm **(A)**; 10 µm **(C)**; 5 µm **(B, D–I)**.

Figs 7.A–O. Light micrographs of *Ostreopsis* cells with different morphologies used for single-cell PCR analyses. Codes of each isolate (IFR-) and origin sample (see Table 1) are given in the lower left corner. **A:** Morphotype 1 (*O.* cf. *ovata*); **B–E:** Morphotype 2 (*O. lenticularis*); **F–J:** Morphotype 3 (*O. siamensis*); **K–O:** Morphotype 4 (*O. heptagona*), note that specimen IFR17-685 (**N**) was infected by *Amoebophrya* sp. Bars = 20 µm.

Fig. 8. Maximum-Likelihood phylogenetic tree based on 189 concatenated sequences of ribosomal operon (SSU + ITS + LSU D1-D3 and D8-D10) (6382 aligned characters) of different strains of Ostreopsidoideae and other gonyaulaceans as outgroup. *Alexandrium/Centrodinium* subclades are collapsed for readability (Full tree in supplementary figure S2). Sequences acquired in the present study are indicated in bold type. Branch robustness was indicated by bootstrap values (ML) and posterior probabilities (BI). Bootstraps values below 65 and posterior probabilities below 0.9 are shown with '-'. On the right, vertical bars delimit major clades corresponding to the different species/genotypes.

Figs 9 A–F Light micrographs of Lugol-fixed *Ostreopsis* cells infected by the parasitoid *Amoebophrya* sp. **A–D:** Cells of *O. lenticularis*, note that three specimens have been used for sequencing the parasitoid (isolate codes indicated in the lower left corner). **E–F:** Cells of *O. heptagona*. The white arrowheads show the more or less developed trophont stage of *Amoebophrya* within *Ostreopsis* cells. Bars = 10 µm.

Fig. 10. Maximum-Likelihood phylogenetic tree based on 49 sequences of small ribosomal SSU and internal transcribed spacer 1 (2354 aligned characters) of *Amoebophrya* spp. and parasitoid dinoflagellates (Syndiniales). The clade including the four new sequences found in infected *Ostreopsis* cells (in bold type) is highlighted with a grey background. Branch robustness was indicated by bootstrap values (ML) and posterior probabilities (BI). Bootstraps values below 65 and posterior probabilities below 0.9 are indicated with '-'.

Credit Author Statement

Aurélie Boisnoir : Conceptualization, Investigation, Ressources, Investigation, Writing – Original Draft, Writing – Review and Editing**; Gwenael Bilien**: Methodology, Validation, Formal Analysis, Ressources, Data Curation, Writing – Review and Editing, **Rodolphe Lemée:** Conceptualization, Writing – Review and Editing, Funding Acquisition, **Nicolas Chomérat:** Conceptualization, Validation, Formal Analysis, Ressources, Data Curation, Writing – Original Draft, Writing – Review and Editing, Visualization, Supervision, Project Administration, Funding Acquisition

Figure

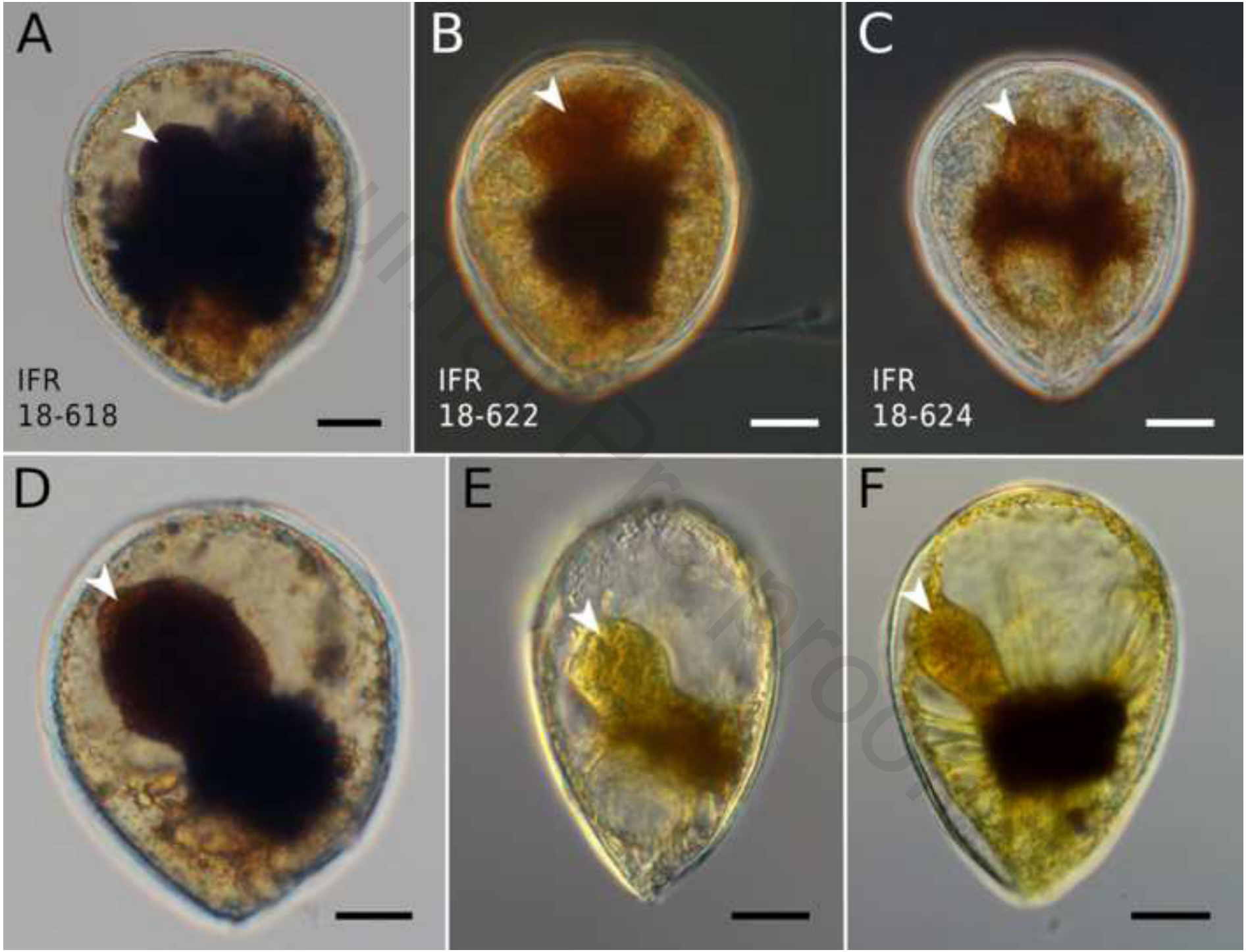

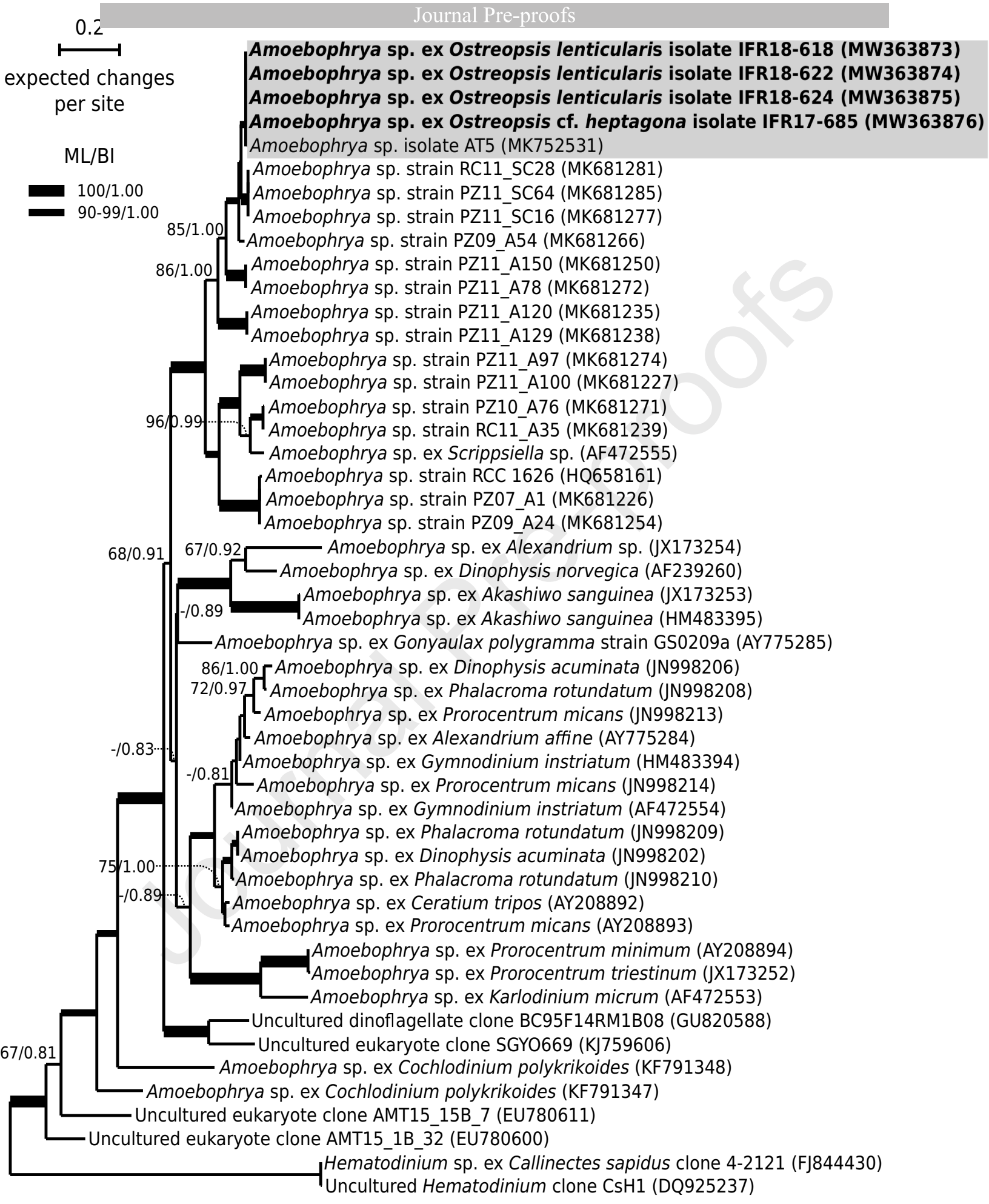

Figure2

Click here to access/download;Figure;Fig2_col.eps

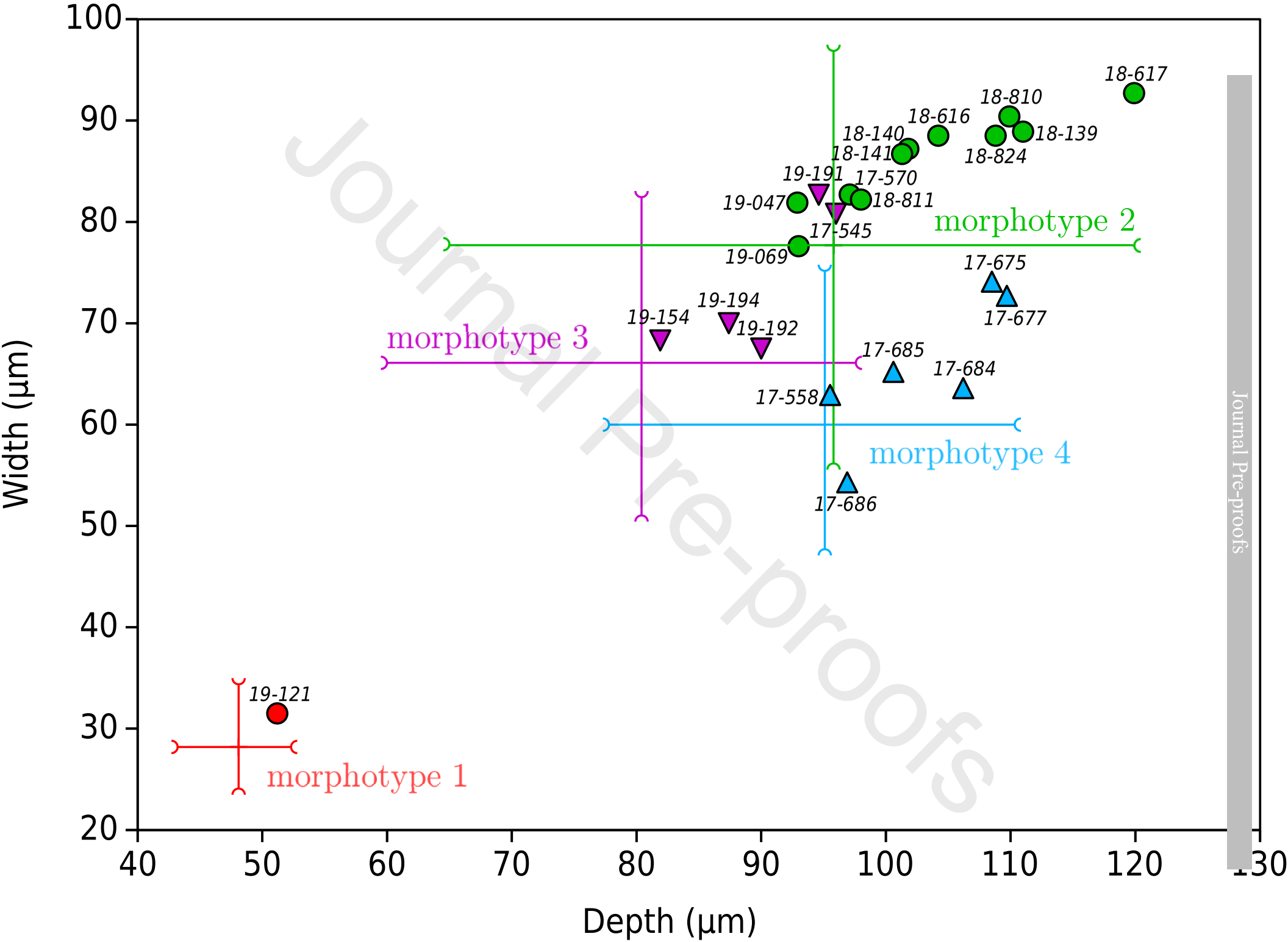

Arri^¤re-plan

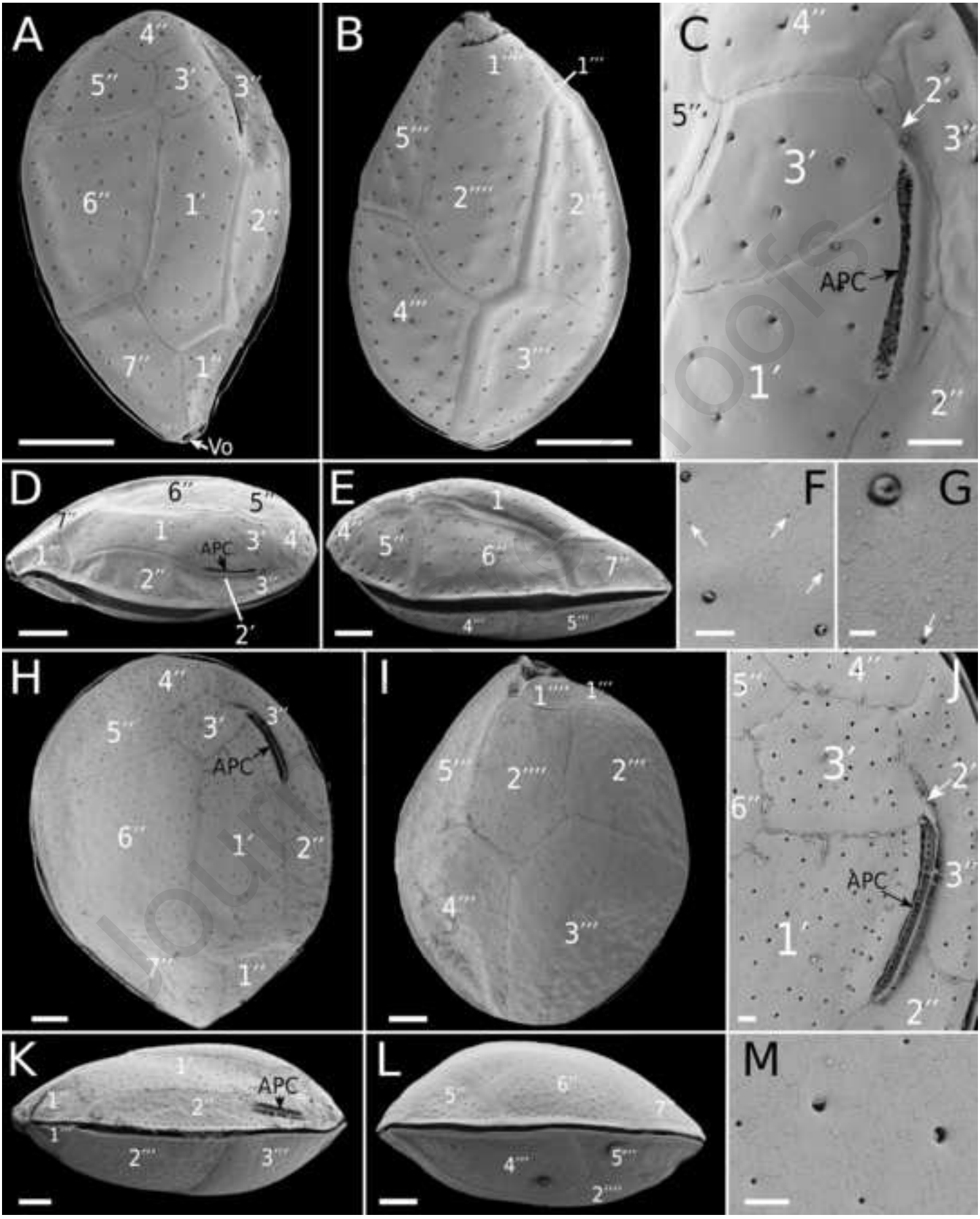

Arri^¤re-plan

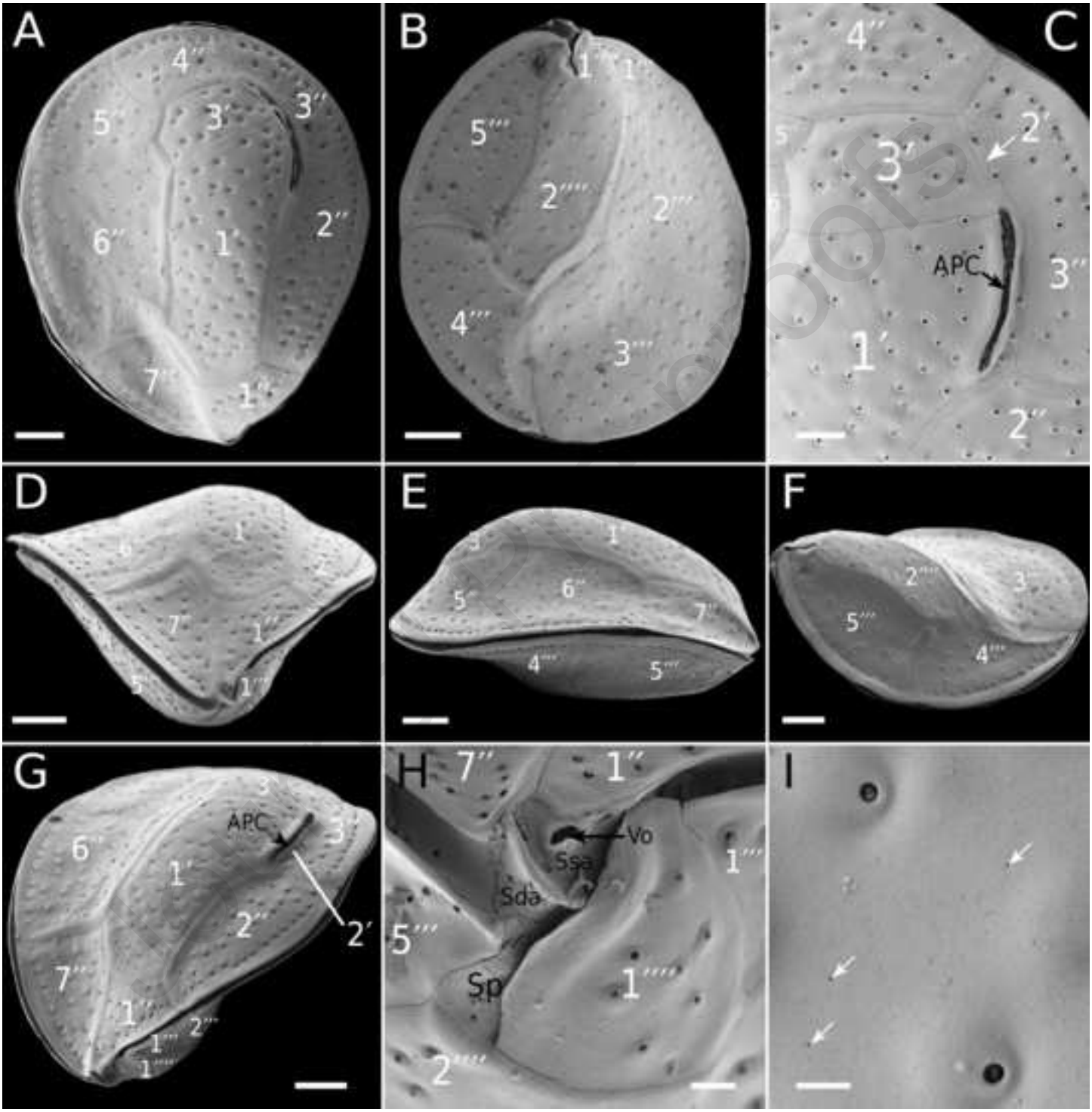

Arri^¤re-plan

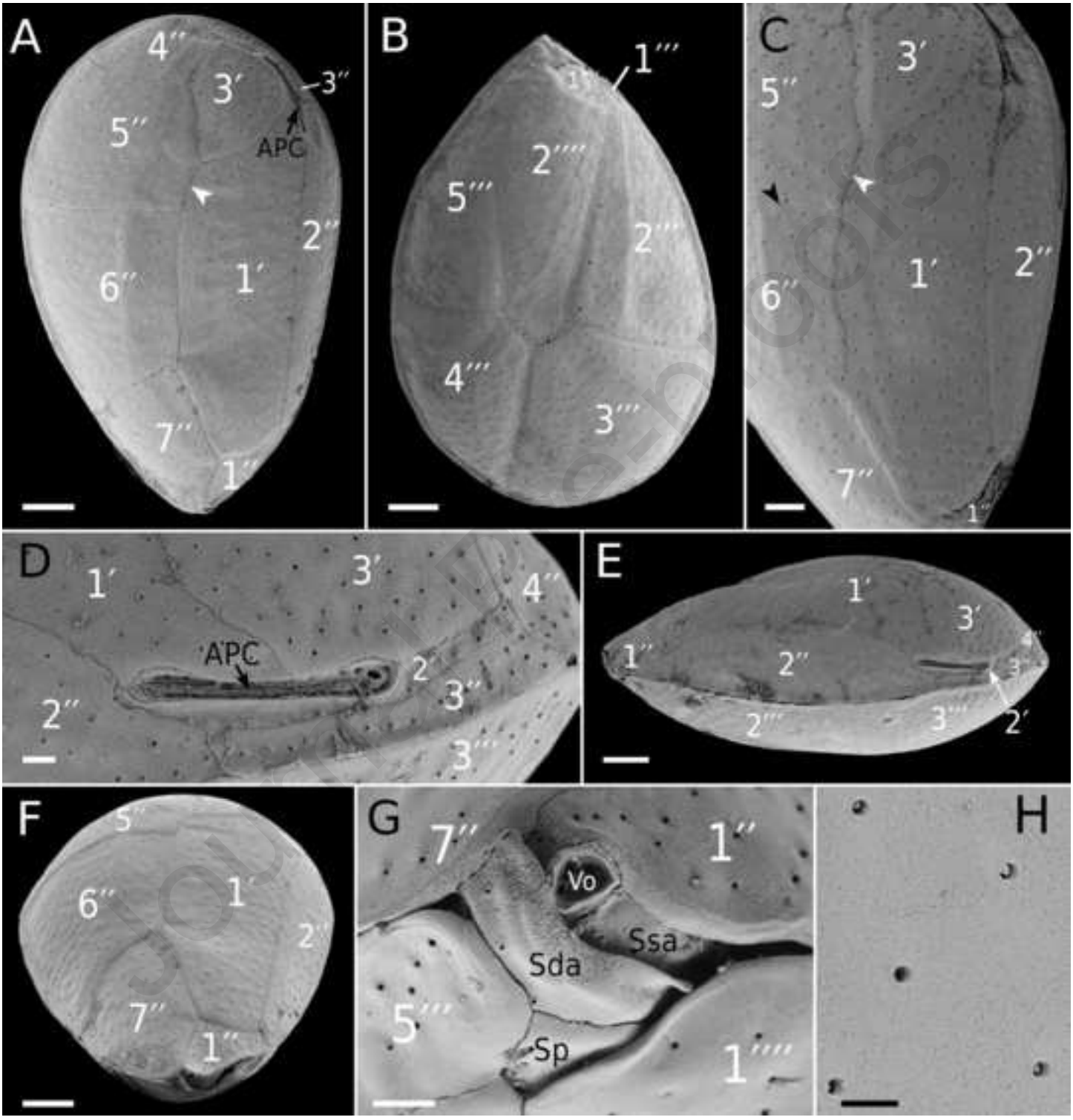

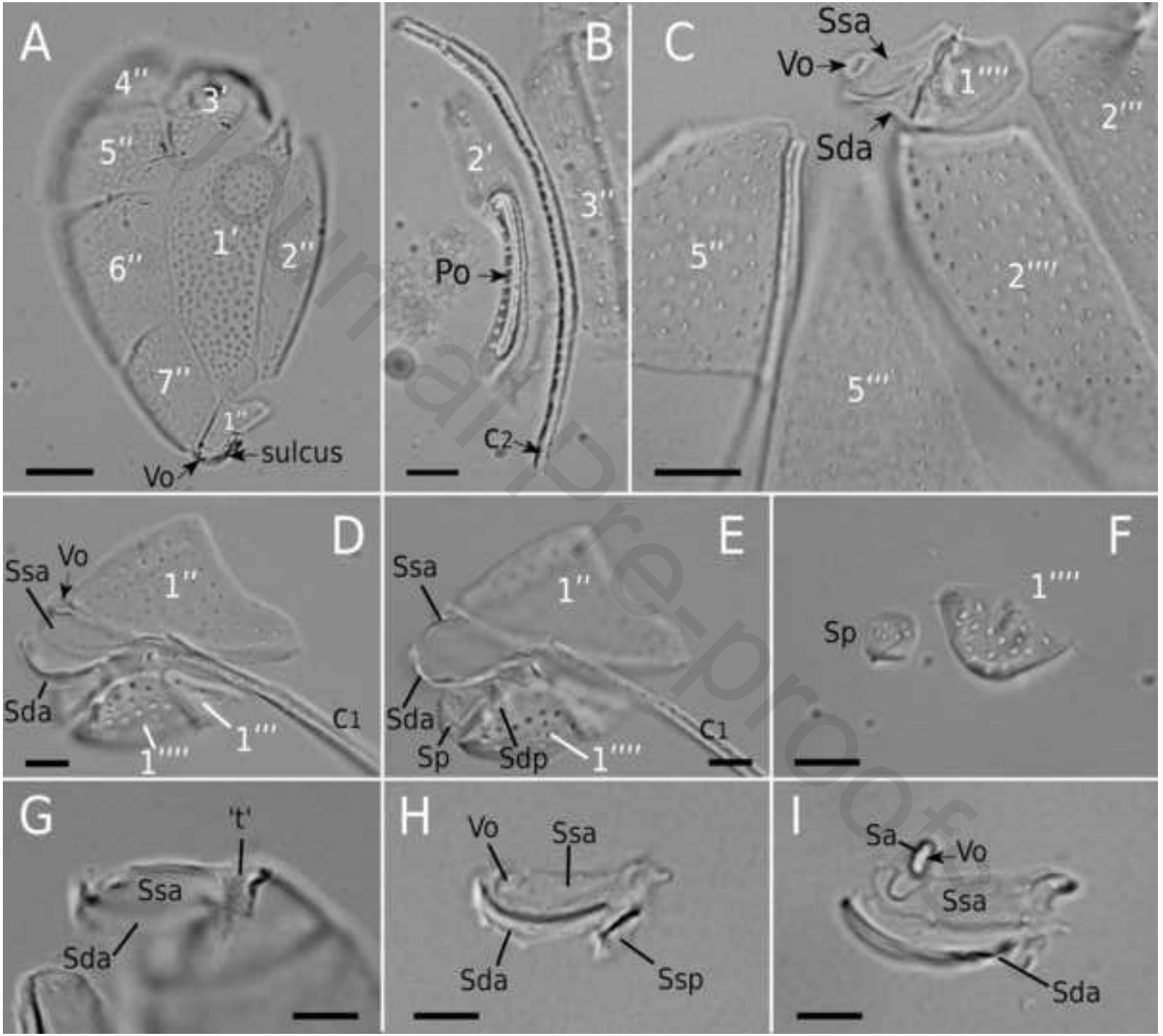

epitheca

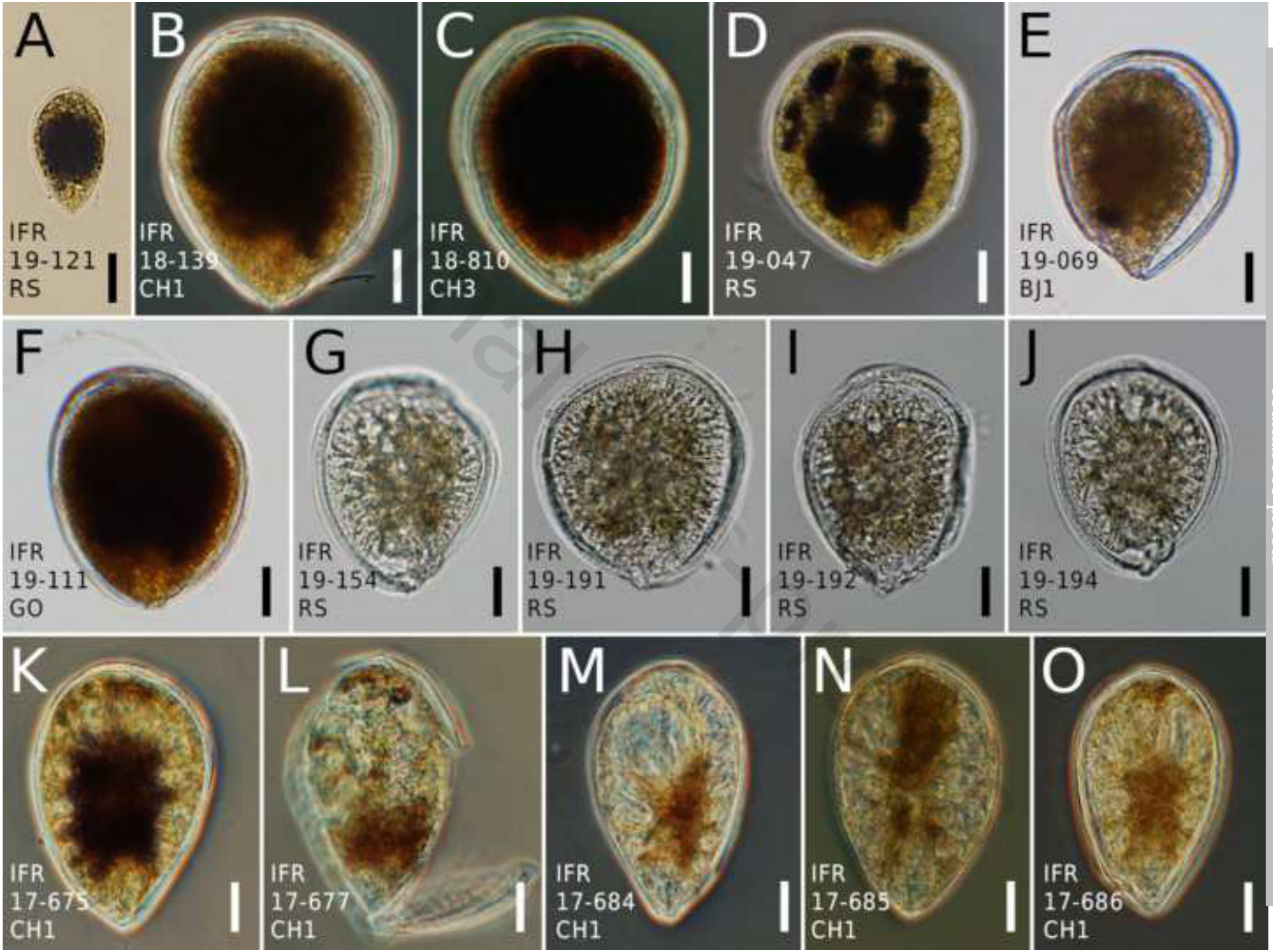

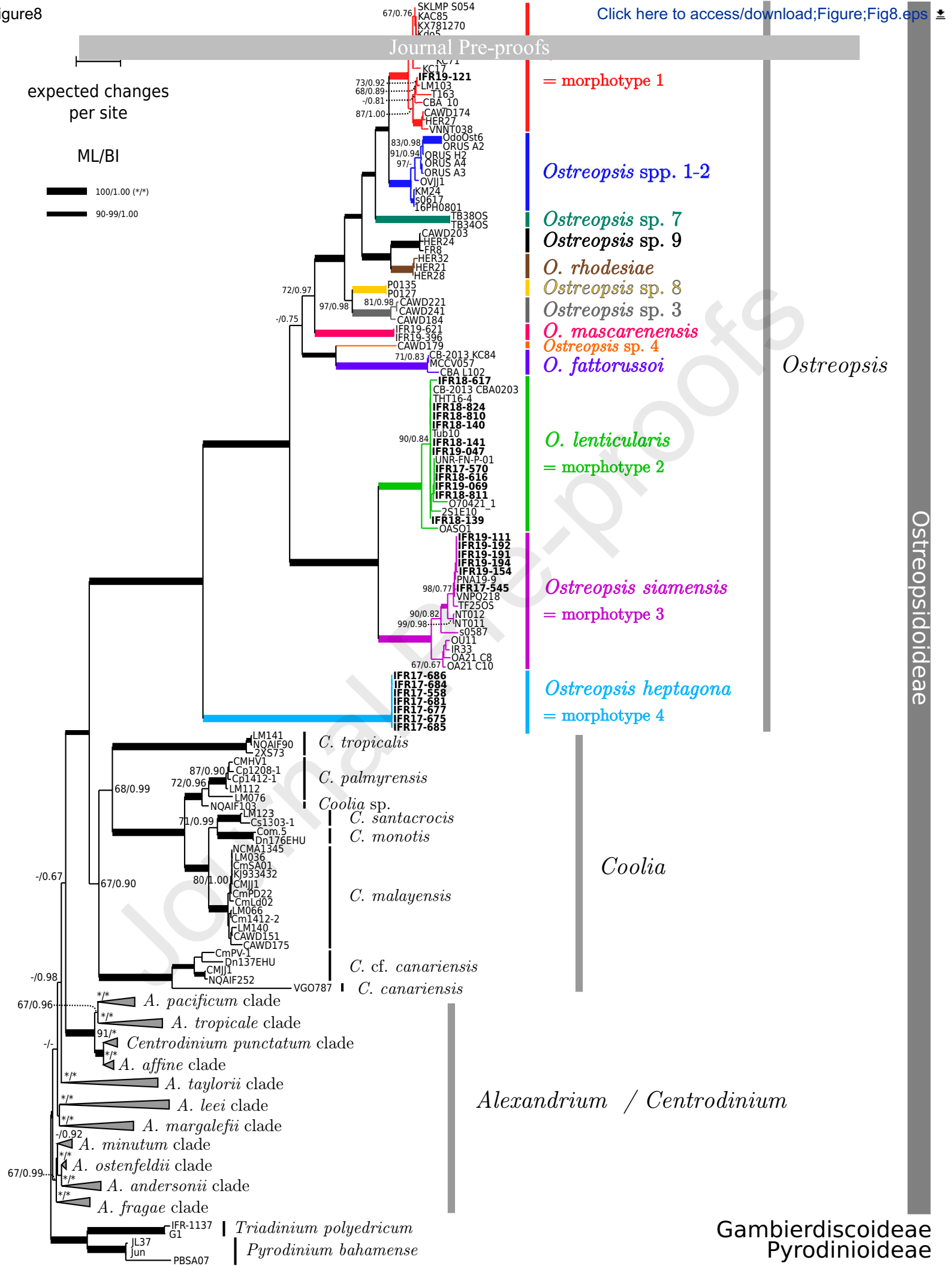

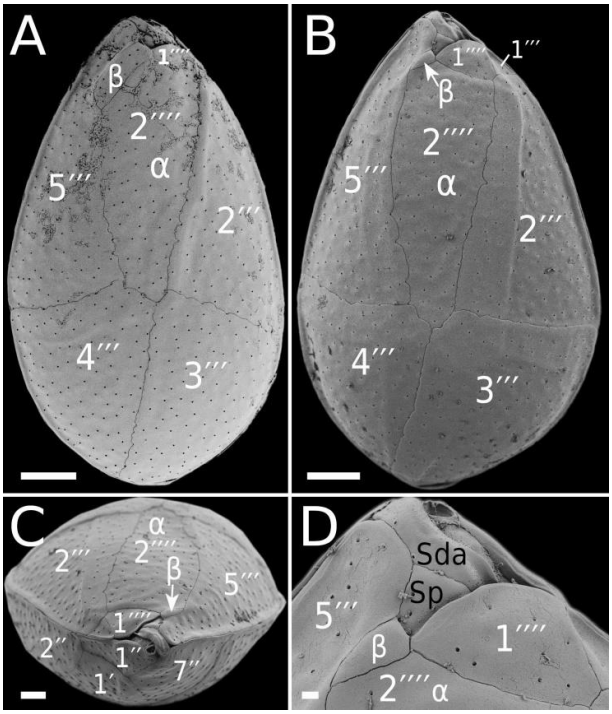

Fig. S1 SEM micrographs of morphotype 4 (*O. heptagona*) from Chapelle showing variations in the thecal plate pattern. **A:** Antapical view of a specimen with the 2⁗ plate divided (α and β). **B:** Antapical view of another specimen with a split 2⁗ plate, with a small part β. **C:** Ventral view of the same specimen with a small plate 2⁗ β. **D:** Detail of the split 2⁗ plate and relations with the sulcal area. Bars: 10 µm **(A–C)**, 1 µm **(D)**.

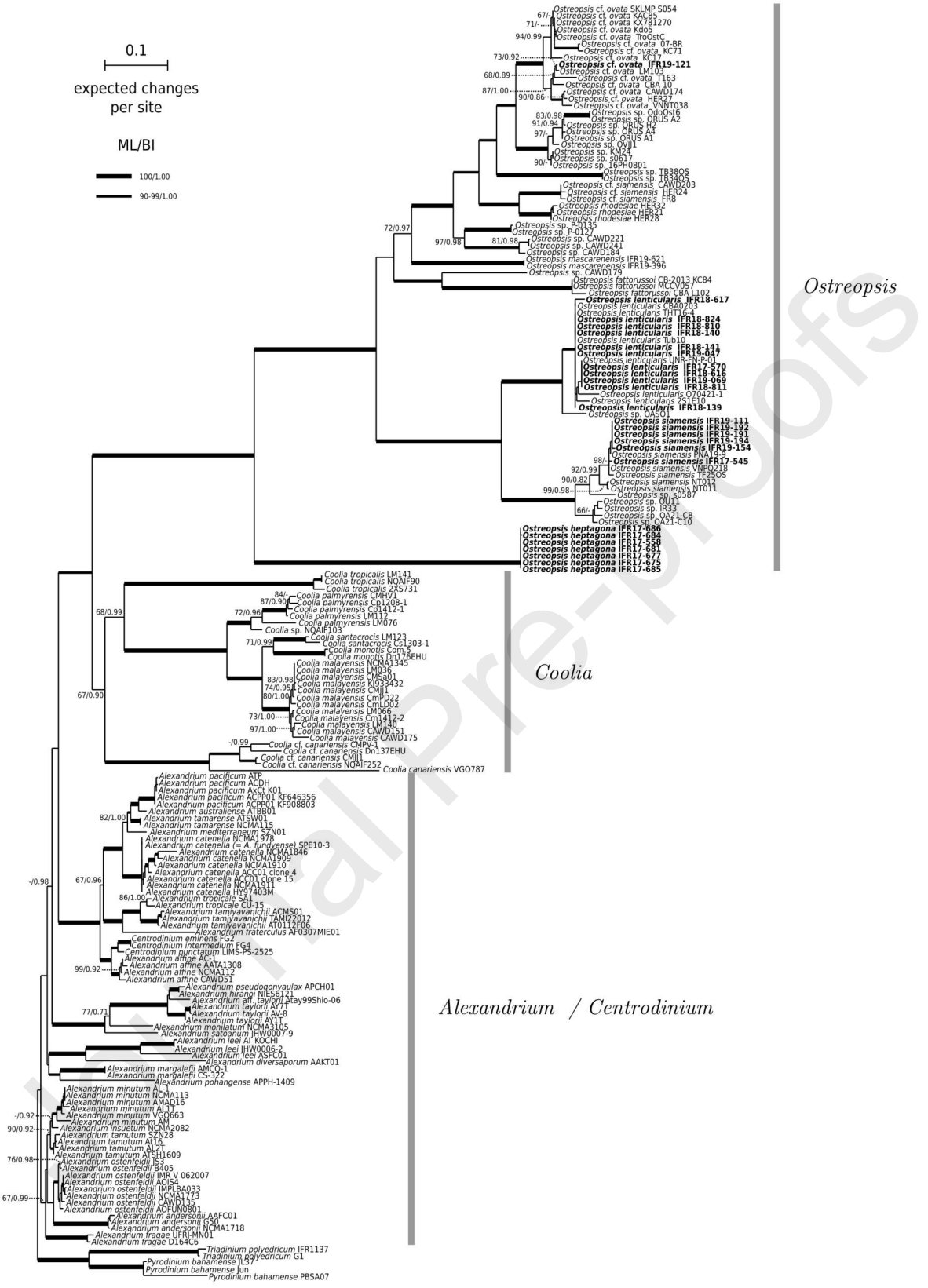

Fig. S2. Maximum-Likelihood phylogenetic tree based on 189 concatenated sequences of ribosomal operon (SSU + ITS + LSU D1 -D3 and D8-D10) (6382 aligned characters) of different strains of Ostreopsidoideae and other gonyaulaceans as outgroup. Sequences acquired in the present study are indicated in bold type. Information on strains and reference of sequences used in the analysis are given in the voucher list (Suppl. Table S2). Branch robustness was indicated by bootstrap values (ML) and posterior probabilities (BI). Bootstraps values below 65 and posterior probabilities below 0.9 are shown with '-'. On the right, vertical bars delimit major clades corresponding to the different genera of Ostreopsidoideae.

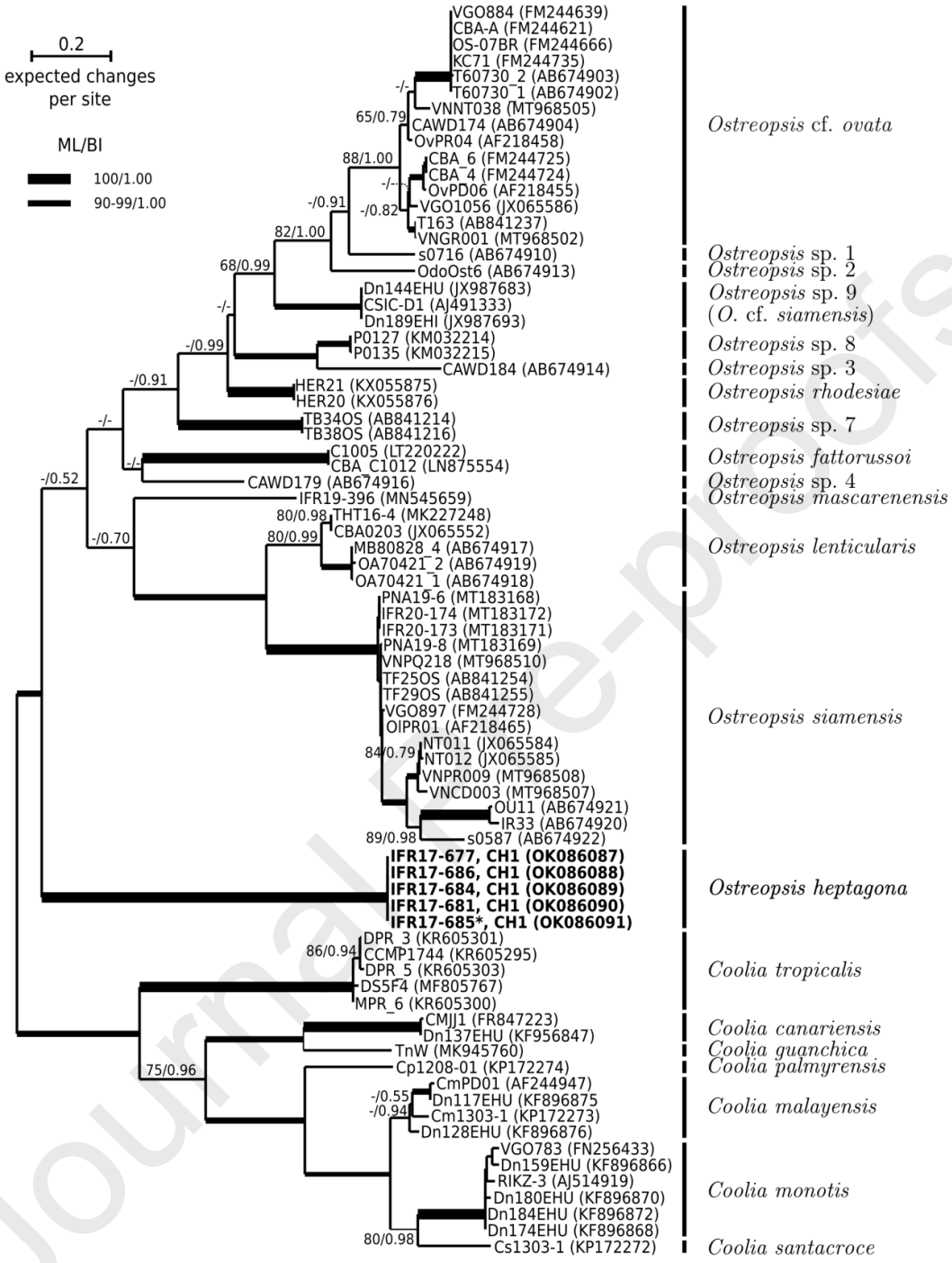

Fig. S3. Maximum-Likelihood phylogenetic tree based on 77 sequences of internal transcribed spacer 1, 5.8S rRNA gene and internal transcribed spacer 2 (ITS region) of different strains of *Ostreopsis* spp. (57 sequences) and *Coolia* spp (20 sequences). Sequences were aligned using MAFFT (q-ins-i option) software (Katoh and Standley, 2013) and ambiguously aligned positions were removed using Gblocks v.0.91b (Castresana, 2000). The final matrix included 577 characters. Sequences acquired in the present study are indicated in